

## Article

# Impact of Climate Change on the Stability of the Miacher Slope, Upper Hunza, Gilgit Baltistan, Pakistan

Mehboob ur Rashid <sup>1,2,3</sup>, Waqas Ahmed <sup>2</sup>, Ihtisham Islam <sup>2,4</sup> , Petros Petrounias <sup>5,6</sup> ,  
Panagiota P. Giannakopoulou <sup>5</sup> and Nikolaos Koukoulas <sup>6,\*</sup>

<sup>1</sup> Geoscience Advance Research Labs, Geological Survey of Pakistan, Islamabad 44000, Pakistan; mehboobgeo89@uop.edu.pk

<sup>2</sup> National Center of Excellence in Geology, University of Peshawar, Peshawar 25130, Pakistan; waqas.nce@uop.edu.pk (W.A.); ihtisham.islam@sbbu.edu.pk (I.I.)

<sup>3</sup> Graduate School of Science and Engineering, Kagoshima University, Korimoto 1-21-35, Kagoshima 890-0065, Japan

<sup>4</sup> Department of Geology, Shaheed Benazir Bhutto University Sheringal, Dir Upper 18050, Pakistan

<sup>5</sup> Section of Earth Materials, Department of Geology, University of Patras, 26504 Patras, Greece

<sup>6</sup> Chemical Process & Energy Resources Institute, Centre for Research & Technology Hellas (CERTH), 15125 Athens, Greece

\* Correspondence: koukoulas@certh.gr

**Abstract:** Especially in recent years, the study of landslide phenomena is considered as very important because of the effects of climate change. The aim of this paper is to examine the stability of the slope located in Miacher Nagar village along the Hunza River (HR), using the Limit Equilibrium Method (LEM). The Miacher slope rises to a height of 900 m from the foot of the Hunza River and has a base angle of 50 degrees. Meta-sediments and quaternary recent glaciated deposits make up the majority of the slope's composition. The slope movement of Miacher was first triggered in 1995, and was further triggered in 2010 and 2013. The slope was geologically, geomorphologically, geotechnically and geochemically investigated as well as modeled by Slope/w to determine the safety factor. Soil samples were analyzed for their geotechnical, geological and geomorphological properties. The Limit Equilibrium Method (LEM) was employed in this study to analyze the Factor of Safety (FOS) of the slope, based on assumptions of the Morgenstern and Price, Ordinary, Janbu and Bishop Methods, using the Slope/w software. Various factors, including pore water pressure, unit weight, cohesion, angle of internal friction and overburden, were examined by analyzing different scenarios. The findings showed that an increase in cohesion and angle of internal friction resulted in an increase in FOS, whereas an increase in unit weight and overburden caused a decrease in FOS. The influence of pore water pressure was positive to a certain extent, but a further increase led to a significant reduction in FOS. The results showed that the Miacher slope is currently stable, as all FOS values were greater than one, based on the existing strength parameters and simulated results obtained using Slope/w.

**Keywords:** probability analysis; shear strength; pore water pressure; factor of safety; Slope/w software; precipitation



**Citation:** Rashid, M.u.; Ahmed, W.; Islam, I.; Petrounias, P.; Giannakopoulou, P.P.; Koukoulas, N. Impact of Climate Change on the Stability of the Miacher Slope, Upper Hunza, Gilgit Baltistan, Pakistan. *Climate* **2023**, *11*, 102. <https://doi.org/10.3390/cli11050102>

Academic Editors: Nir Y. Krakauer and Talib E. Butt

Received: 13 March 2023

Revised: 4 May 2023

Accepted: 5 May 2023

Published: 8 May 2023



**Copyright:** © 2023 by the authors. Licensee MDPI, Basel, Switzerland. This article is an open access article distributed under the terms and conditions of the Creative Commons Attribution (CC BY) license (<https://creativecommons.org/licenses/by/4.0/>).

## 1. Introduction

The failure of earth slopes is a natural occurrence that is triggered by the gravitational movement of the materials that make up the slope. These materials can be rocks, soils, artificial fill or a combination of these [1]. The rate of movement of these materials can range from very slow to extremely rapid, leading to disastrous consequences [2]. Slope failure occurs when the disturbing force becomes greater than the resisting force, caused by a loss in the soil strength [3]. Slope failure susceptibility depends on a number of factors

such as slope angle, lithology, land cover, precipitation, drainage pattern, groundwater setting and thickness of overburden [4–11].

Pakistan is located in a region with high seismic activity and experiences heavy rainfall, especially in its northern areas such as Kashmir, Murree, Muzaffarabad, Gilgit, Hunza, Chitral and Swat [12–19]. According to Khan [20], about 30% of the world's landslides occur only in Himalayan ranges with an average damage of USD 1 billion year<sup>-1</sup>, added to death casualties of 200 year<sup>-1</sup> [21–23]. The erosion rate in both Karakorum and the Himalayas is about 0.2 mm to >10 mm year<sup>-1</sup> responsible for steep slopes, and with deposition of thick valley fills >700 m of weathered and eroded materials from unstable slopes [24,25]. The upper Hunza basin in the Karakoram Range has been reported to have higher rates of erosion [24]. The Hunza area is well-known for avalanches, debris flows, torrential slides and floods [26–32]. The noticeable events of calamitous occasions in locales of the Himalayan Karakorum region are the 1972 mud flow in upper Hunza, the 1974 Shishkit event BaltBar Valley mud flow with slurry avalanche, the 1977 Darkot and upper Yasin debris avalanche and the 2010 Attabad debris landslide. During the International Karakoram Expedition of 1980, a detailed survey was conducted along a 139 km stretch of the Karakoram Highway between Gilgit and Gulmit. The survey revealed evidence of 335 landslides of different types, sizes and ages [32–34]. The scars of displaced slopes, debris flows and large alluvial fans provided evidence of these events [35]. In some cases, the displacement of a large amount of debris can cause blockage of the river, leading to devastating flooding downstream [36–38].

Yafeng and Wenying [39] reported that the Shishkit event of 1974, which originated from the BaltBar Valley of upper Hunza, involved the rapid movement of approximately 5 million m<sup>3</sup> of mud-rock slurry at a speed of 6300 m s<sup>-1</sup>. In addition, Hewitt [34,40] documented a catastrophic deposition of around 20 × 10<sup>6</sup> m<sup>3</sup> of debris on the Baltar glacier in the Karakoram in July of 1986. Flash floods, glacier-lake outbursts, landslides and mudflows also contribute to the region's substantial transport of weathered material. The Himalayan Karakoram Region is known for occurrences of avalanches, debris flows and torrential slides, and such catastrophic events are common in these areas. The mudflow, debris avalanche debris flow and all associated types of slope failure are influenced by the effect of precipitation [6,7,9,41–45]. Intense rainfall is a major contributor to the occurrence of landslides since it raises the groundwater table, increases the pressure inside the soil pores and negatively affects the slope's stability [46,47]. Porosity, density, water content, saturation level and permeability are all characteristics that can affect shear strength and are all strongly correlated with rainfall. Short-duration, high-intensity rainfall can alter intergranular friction and effective stress [7,44].

Over the past thirty years, numerous floods have been caused by landslides or the breaking of dams created by debris flows in the Hunza area. The following is a list of some of these events, compiled from various sources. According to Miller [33], in 1972/3, there was a mudflow that occurred after 10.3 mm of rainfall in two days, which led to the blocking of the Hunza River at Batura. The flooding caused by the mudflow in 1973 led to damage to the highway and bridge over the Batura channel, which is mentioned in the introduction to the glaciological study of the Batura glacier by Yafeng and Wenying [39]. A mudflow with a front 20 to 30 m high occurred from Baltbar Nallah on the left bank tributary 18 km south of Batura on 11 April 1974 [39]. The mudflow from Baltbar Nallah in 1974 created a fan that was 300 to 400 m wide, over 150 m long and 80 to 100 m high, which blocked the Hunza River and submerged the Friendship Bridge constructed in 1970, resulting in the formation of a lake that was 12 km long [48]. On 14 August 1974, at Baltbar Nallah, the debris flow had a front of 5 m high and the river stage rose rapidly, submerging the bridge over the Hunza. One hour later, the river cut through the fan deposits [48]. The devastating account of a flood in 1977 in the village of Darkot in Upper Yasin was caused by a mixture of rocks and mud that destroyed the entire village and all of the farmland. It is a tragic reminder of the destructive power of natural disasters in this region [49].

Landslides have historically caused devastation in the Hunza region and are infamous for occurring [33,34,39,40,48,49]. There is a lot of continuing new research. Hunza is primarily focused on using remote sensing methods to comprehend how to identify and understand the mechanism of newly created landslides [26,28]. Accessing the landslide in the Hunza region also made use of non-intrusive geophysical tools such as electrical resistivity soundings (ERS) and ground penetrating radar (GPR) [27]. Some researchers have used a GIS tool to analyze satellite imagery to create a map of the Hunza Nagar region's landslides [30,31]. Some research projects use remote sensing techniques to analyze the Attabad landslide dam [12]. Most research, in general, concentrates on using remote methods to analyze landslides in the study region; no work has been conducted on geotechnical investigation of soil samples or estimating the likelihood of failure.

The Hunza River is an important water source for irrigation in the downstream areas, particularly in the Hunza and Gilgit valleys, well-known for their fruit orchards and vegetable farms. The Hunza river also has significant hydropower potential, with several small and large hydropower projects already operational or under construction. The water of the Hunza River is also used for drinking and domestic purposes in the surrounding areas. On 4 January 2010, a sudden avalanche caused a massive landslide that dammed the Hunza River at Attabad, creating a lake that extended over 23 km upstream and displaced thousands of people. The landslide resulted in the formation of a large unstable Attabad Lake with an extension of 21 km and a depth of 109 m and having an inflow rate of  $419 \text{ m}^3 \text{ s}^{-1}$  against the outpouring of  $358 \text{ m}^3 \text{ s}^{-1}$ , posing a significant threat to the downstream communities in case of a catastrophic failure of the dam. The incident also cut off the Karakoram Highway, the main trade route between Pakistan and China, causing significant economic losses to the region [38].

To accurately assess the risk of a landslide, it is important to consider the potential for an event to occur with a certain magnitude or force within a specific time frame. This requires careful analysis of the geological and environmental conditions of the area, as well as an understanding of the potential triggers for landslides such as heavy rainfall and seismic activity. By evaluating these factors, experts can develop strategies to mitigate the risk of landslides and minimize their impact on communities and infrastructure [50]. By analyzing past events, tracking records of each landslide and understanding the conditions that led them, we can estimate how often a similar event may occur in the future [51]. The vulnerability of elements at risk is an important task in landslide risk assessment by quantifying the level of damage and risk that may occur from a landslide of a given magnitude [52]. The vulnerability and mitigative measures can be conducted through field surveys, remote sensing techniques and modeling approaches [50–52].

The objectives of the present study are to investigate the probability of slope failure of the Miacher landslide, Hunza-Nagar District, based on the geotechnical approach, effects of precipitation and mineralogy and to evaluate the key factors causing the failure and estimate the probability of failures at present conditions. Study Area:

The study area of Miacher lies between  $36^{\circ}14'32''$  to  $36^{\circ}15'18''$  N latitudes and  $74^{\circ}34'15''$  to  $74^{\circ}33'32''$  E longitudes, within the administrative territory of Upper Hunza Gilgit Baltistan, Pakistan. The village Miacher is cited along the eastern side with an altitude of 780 m from the Hunza River and 2500 m above mean sea level (Figure 1). The study area is the southern extreme of the Karakorum block and is bounded by the Pamir Fault in the north, the Main Karakoram thrust (MKT) in the south, the Karakoram Fault to the east and the Sarobi Fault to the south (Figure 2a) [53–55].

Meta-phyllite and quartzite are the main lithological units in the study area, and they are of Ordovician to late Devonian age [54,56]. These rocks are overlain by silty clayey soil; silty clayey soils are known to have poor stability and are prone to landslides. The weathering of the underlying rock formations results in the formation of silty clay and weakness of the soil, increasing the likelihood of slope failure [56,57] (Figure 2b). The climate of Hunza is generally cold and dry, with temperatures typically ranging from  $-10^{\circ}\text{C}$  to  $25^{\circ}\text{C}$  depending on the season and altitude. Precipitation is low, with an annual

average of around 200–400 mm, and occurs mostly in the form of snow and rain between December and April. During the monsoon season, which occurs from July to September, there is a high risk of mass movements due to increased precipitation and snow melting caused by rising temperatures. This can increase the likelihood of landslides and other types of mass movements.

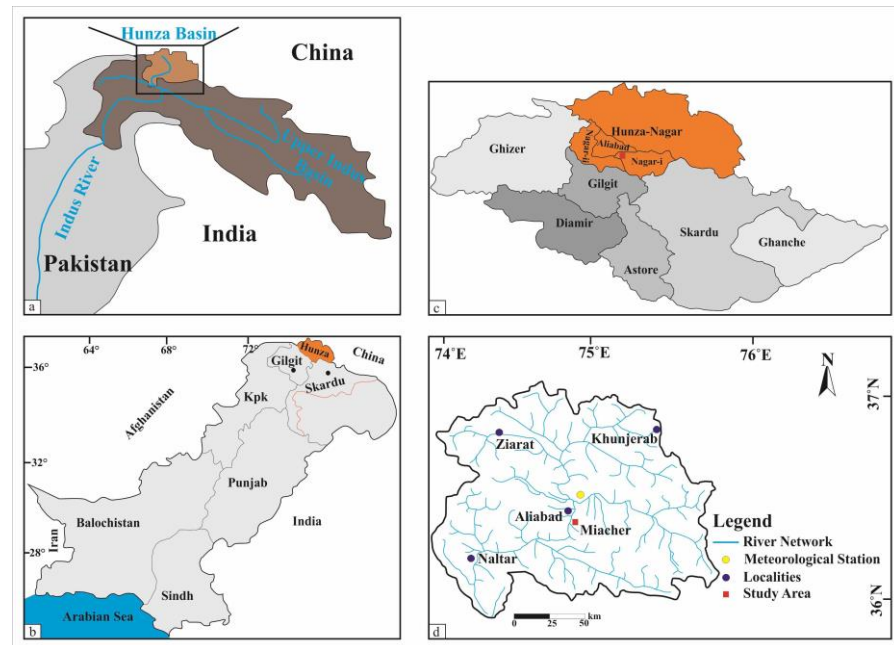


**Figure 1.** Location map of the study area, (a) showing the Hunza basin in Asia, (b) showing the study area in Pakistan, (c) geographical division of Gilgit Baltistan Province, (d) drainage map of Hunza area showing study area and meteorological station for which rainfall data were acquired.

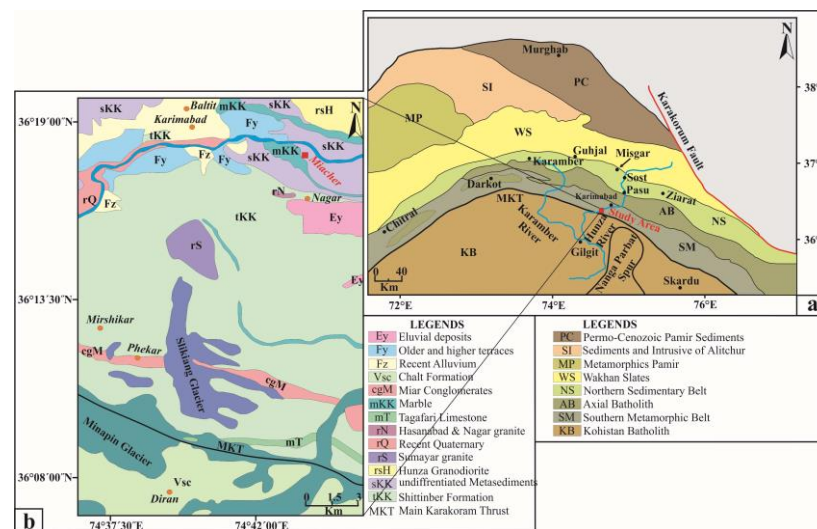


**Figure 2.** (a) Tectonic map of the Hunza showing the study area [54], (b) geological map of upper Hunza showing the study area modified after Le Fort and Pêcher [56].

## 2. Methodology

The slope stability involves the estimation of a factor of safety (FOS) that is based on the geometry of the slope, collection of soil samples, strength properties of soil and modeling of slope using Slope/w to establish FOS (see the flow chart Figure 3). The inherent unreliability and difficulty in the estimation of soil strength parameters using

a trial and error method can be effectively controlled by applying probability and sensitivity analysis of the observed characteristics and properties of the soil mass [58]. In this regard, the methodology is categorized into two steps, i.e., fieldwork and laboratory work. The soil samples were collected as grab and undisturbed from the crest and mid of slope and they were analyzed to identify their geotechnical properties. The geometry of the slope (height, width and slope angle) was determined using a Laser range finder (Nikon, 6/20 with 6–500 m range) and Total Station. The soil properties such as liquid limit (LL), plastic limit (PL), moisture contents ( $\omega$ ), specific gravity ( $G_s$ ) and unit weight ( $\gamma$ ) of the collected samples during the field study were analyzed in the geotechnical laboratory of the National Center of Excellence in Geology. Sieve and hydrometer analyses were conducted for grain size distribution (GSD) using ASTM standards (D421 and D422) (Figure 4). The average LL of the Miacher soil range was 24, with LLs of analyzed samples measuring 23, 24 and 25 (Figure 4a). The mechanical analysis of the soil was conducted using both sieve analysis and hydrometer analysis and was used for the classification of soil given in Figure 4b. The index properties of Miacher soil are summarized in Table 1.

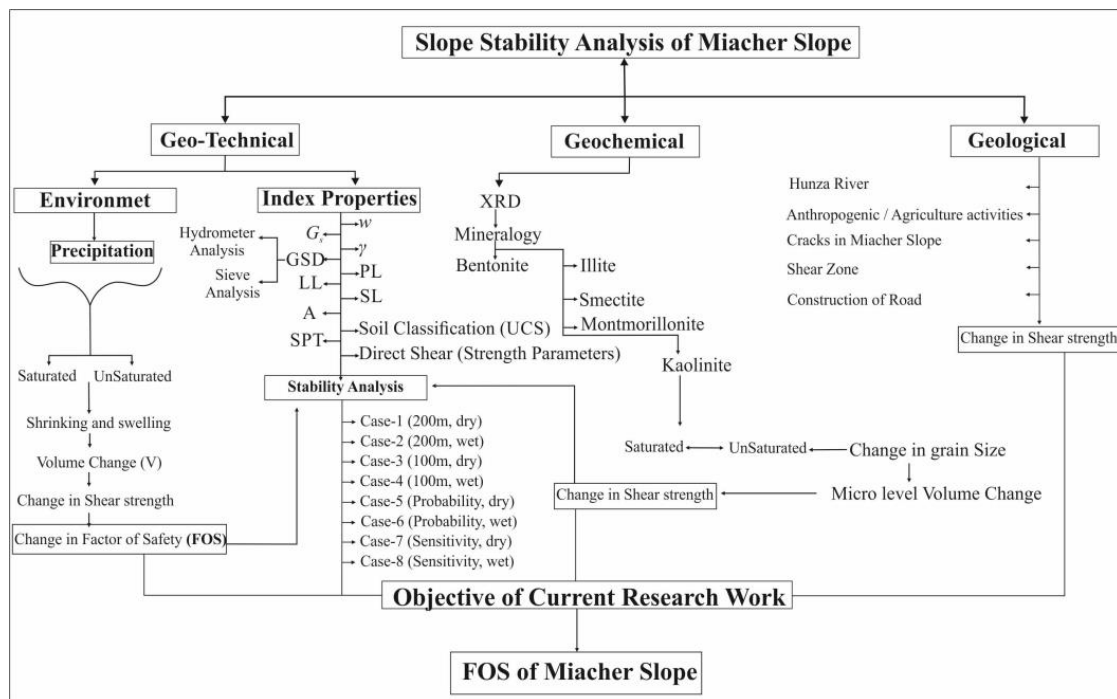


Figure 3. Flow Chart showing detailed methodology adopted for the Slope Stability Analysis of Miacher slope.

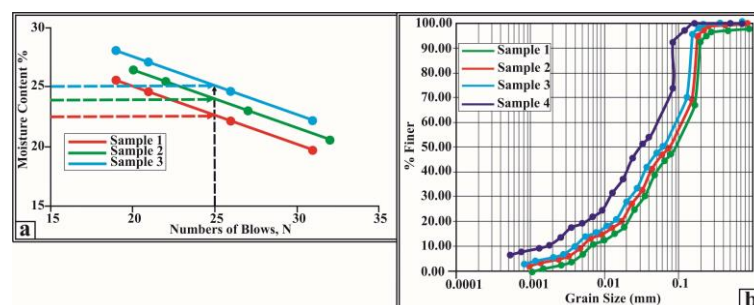
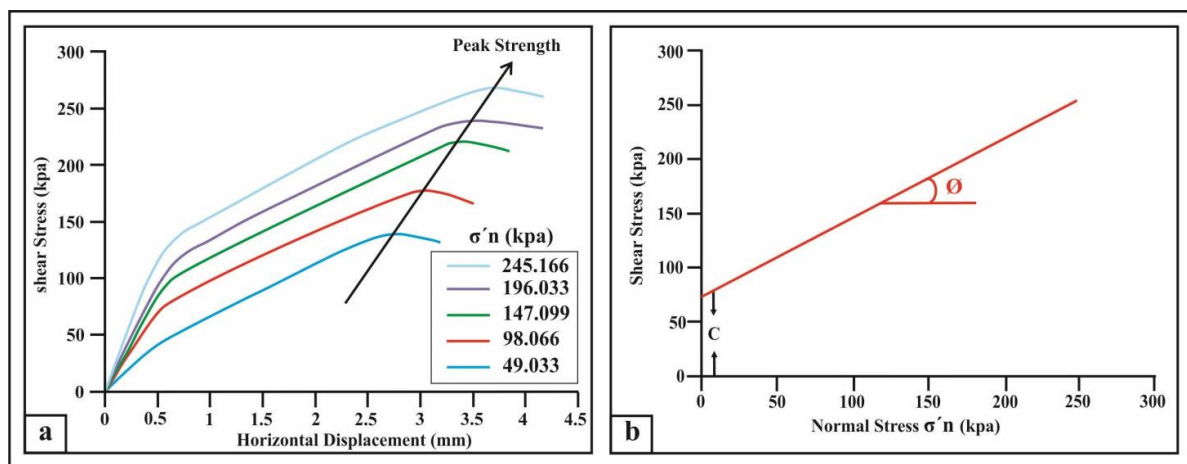


Figure 4. (a) LL test, (b) Index Properties of Miacher soil.

**Table 1.** Showing index properties of Miacher slope soil.

Parameters	Sample 1	Sample 2	Sample 3	ASTM
Moisture Content (%)	1%	1%	3%	D2216
Specific Gravity (Gs)	2.65	2.54	2.68	D854
Liquid Limit (LL)	23	24	25	D4318
Plastic Limit (PL)	21	21	22	D4319
Plastic Index (PI)	2	3	3	D4320
Unit weight ( $\gamma$ )	12 KN/m <sup>3</sup>	12 KN/m <sup>3</sup>	13 KN/m <sup>3</sup>	D2937

For soil geochemistry, X-ray Diffractometer (XRD) was used to determine clay minerals and type of cementing materials. The shear strength parameters, i.e., peak strength, cohesion ( $c$ ) and angle of internal friction ( $\Phi$ ) were determined using direct shear box (ASTM, D3080) [59] (Figure 5). The peak strength of the Miacher soil is given in Figure 5a, showing that with an increase in shear stress, the soil shows shear resistance for a fixed normal stress, reaches a peak value and after that the soil fails. The cohesion and angle of internal friction is 70 and 28 degrees (Figure 5b). The strength parameters are summarized in Table 2.

**Figure 5.** (a) Peak strength of Miacher soil, (b) cohesion and angle of internal friction ( $\Phi$ ) of Miacher soil.**Table 2.** Showing strength parameters of Miacher Soil.

Normal Stress (KPa)	Shear Stress (KPa)	Residual Stress (KPa)	Phi Angle ( $\Phi$ )
49	104	97	43
98	139	128	31
147	174	167	24
196	212	201	21
245	253	243	20
Average			28

The Miacher slope soil was classified according to a unified classification system [60] by taking into consideration the GSD and Index properties (Table 3). Based on the unified classification system, the Miacher slope soil was classified as silty sand having no gravel content, with sand portion of 49% and fine silt and clay of 51% (Figure 6a). The plasticity of soil was also defined using a plasticity index (PI) vs. Liquid Limit (LL) graph, having an average plasticity index of 3 and an LL of 24 (Figure 6b). With these properties, it shows that Miacher Soils fall under the group of low plasticity silt (ML) (Figure 6b).

**Table 3.** USCS chart showing different soil types [60].

Description		Group Symbols	Group Name
<b>Coarse grained Soil</b> >50% soil retained (R) on Sieve # 200	<b>Gravels</b> >50% Coarse fraction R on Sieve # 04	<b>Clean Gravel</b> <5% fines	GW Well graded gravel
			GP Poorly graded gravel
		<b>Gravel + Fines</b> >12% fines	GM Silty gravel
			GC Clayey Gravel
	<b>Sands</b> ≥50% Coarse fraction Passes on Sieve # 04	<b>Clean Sand</b> <5% fines	SW Well graded sand
			SP Poorly graded sand
		<b>Sand + Fines</b> >12% fines	SM Silty sand
			SC Clayey sand
<b>Fine grained Soil</b> ≥50% passes on Sieve # 200	<b>Silts &amp; Clays</b> Liquid Limit (LL) < 50	ML Inorganic	Low plasticity silt
		CL Inorganic	Low plasticity clay
		OL Organic	Low plasticity silt & clay
	<b>Silts &amp; Clays</b> Liquid Limit (LL) ≥ 50	MH Inorganic	Elastic silt
		CH Inorganic	High plasticity clay
		OH Organic	High plasticity clay & silt
Highly Organic		Pt	Peat

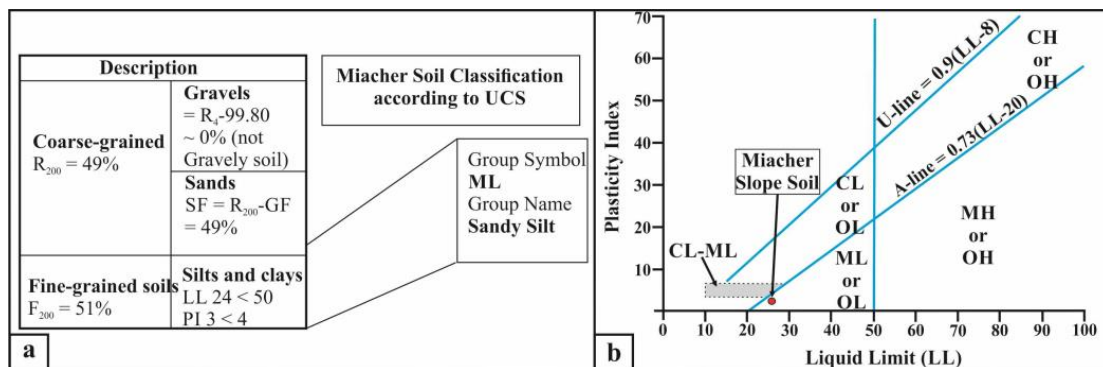


**Figure 6.** (a) Miacher soil classification based on sieve/hydrometer analysis and index properties, (b) plasticity chart of UCS showing position of Miacher slope soil.

The FOS was determined with the limit equilibrium method (LEM) using Slope/w software because of its simplicity and characterization based on both force equilibrium and moment equilibrium principle [61]. The Slope/w incorporates strength properties as  $\Phi$ ,  $c$ ,  $\gamma$  and geometry of slope to establish FOS for Morgenstern and Price, Bishop, Ordinary and Janbu methods with surface characterization. The Miacher slope is divided into two layers with loose top materials of low plasticity silt and subsurface layer of bedrock of metamorphic meta-sediments (Figure 7). The parameters adopted for analysis in Slope/w were the angle of internal friction, cohesion, unit weight, specific gravity, parameters of the slope, thickness of loose top materials and weather condition (dry and wet).

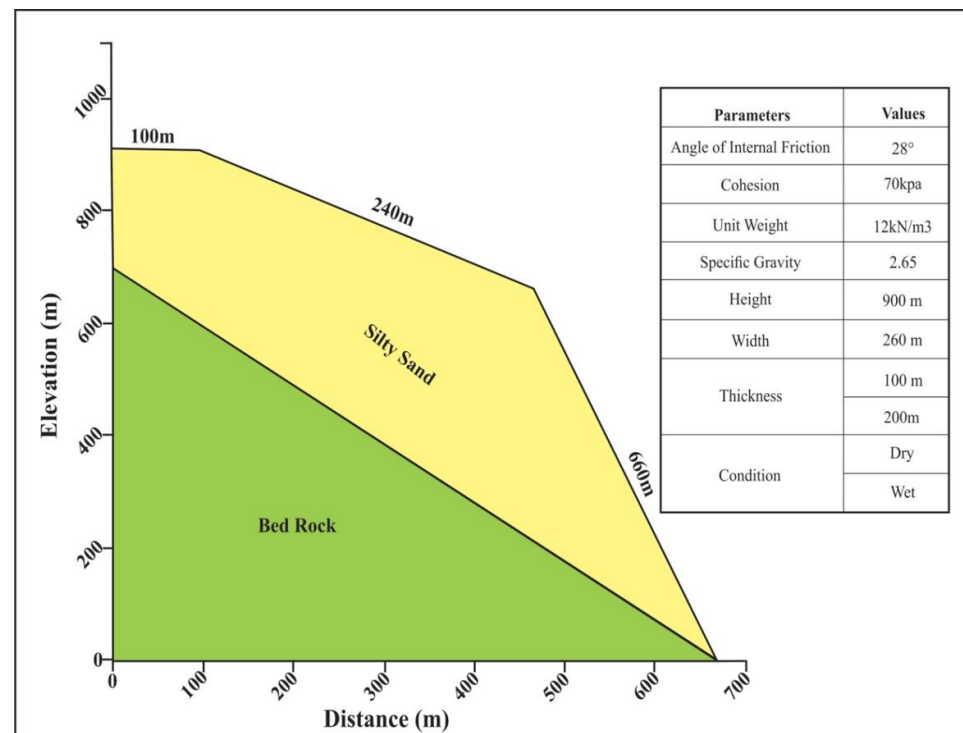


**Figure 7.** Miacher slope model with different parameters used during slope modeling.

### 3. Results and Discussion

#### 3.1. Slope Stability Evaluation

The Miacher slope was analyzed with Limit Equilibrium Methods (LEM) using Slope/w 2002 (GeoSlope International Ltd., Calgary, Canada) [38]. The present study was conducted in order to examine the slope stability under the natural conditions (dry and wet conditions and overburden) that may influence the slope stability in future. The FOS was computed for Janbu generalized (JG), Morgenstern and Price (MP), Bishop's simplified (B) and Ordinary (O) procedures of obeying the principle of LEM. The Entry and Exit option was selected to regulate the critical slip surface (CSS) and approach of failure.

Input parameters used in slope stability analysis are based on field and laboratory measurements, which are always subject to some degree of uncertainty. Monte Carlo probabilistic analysis was adopted by considering the variability and uncertainty associated with input parameters. The Monte Carlo simulation then randomly samples from each input parameter's distribution to generate multiple combinations of input parameters, which are used to run the slope stability analysis multiple times. This results in a distribution of possible outcomes, allowing for a better understanding of the uncertainty and risk associated with the slope stability analysis (Figure 7). The probability of failure and reliability index was then calculated for the Miacher slope with the distribution of the Factor of Safety (FoS) along the slope for different LEMs.

#### 3.2. Analysis of Miacher Landslide

Case One: Thickness 200 m and dry season

In the first case, the slope was analyzed by taking the assumption of dry conditions and a thickness of 200 m as overburden. The FOS for the said conditions was computed by employing the selected parameters in Slope/w; the simulation results showed the CSS (Figure 8a).

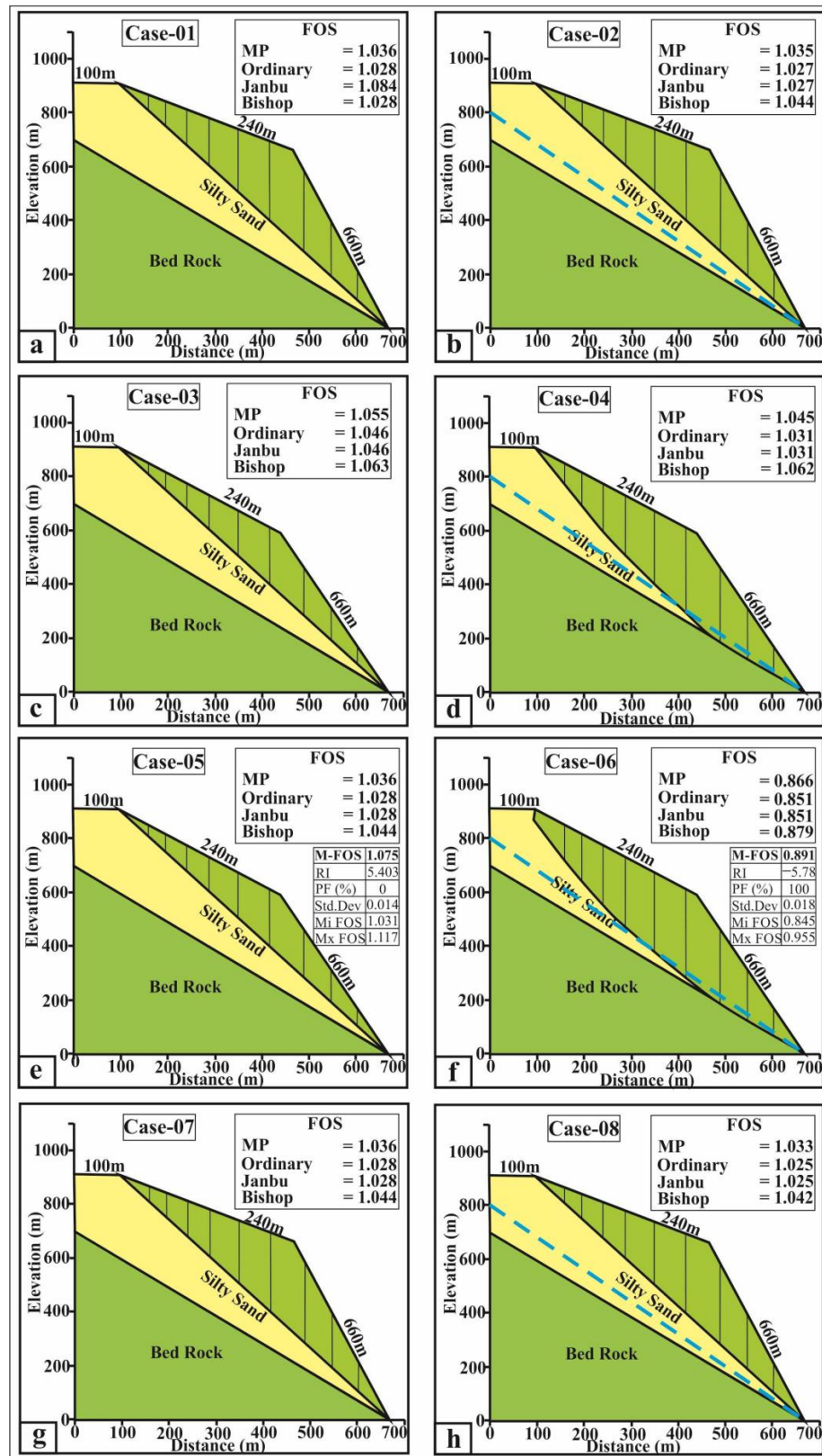


**Figure 8.** (a–h). FOS of different Cases 1–8, assumed for Miacher slope modeling. (RI = Reliability Index, PF = Probability of Failure, Std. Dev = Standard Deviation, Mi FOS = Minimum Factor of Safety, Mx FOS = Maximum Factor of Safety, M-FOS = Mean Factor of Safety).

The comparison of different strength and stress parameters that affect slope stability can help to determine the most critical factors and their impact on the Factor of Safety (FOS), which have also been plotted and analyzed. The peak value of frictional and effective normal stress was 4000 kPa and 2500 kPa, having a difference of 1500 MPa and represented by frictional strength stability (Figure 9a). The difference between shear strength and shear mobilized was 500 kPa, showing a positive effect on stability as shear strength is greater than mobilized strength (Figure 9b). The interslice normal force had a peak value of 12,000 kN, while Interslice shear force reached a peak value of 2000 kN with a total difference of 10,000 kN, resulting in increasing the interslice stability of the soil (Figure 9c). The strength parameters (frictional and shear strength and interslice normal force) in Case one were greater than the destabilizing forces (normal stress, shear mobilized and interslice shear force), showing the strength of the Miacher slope in the mentioned conditions.

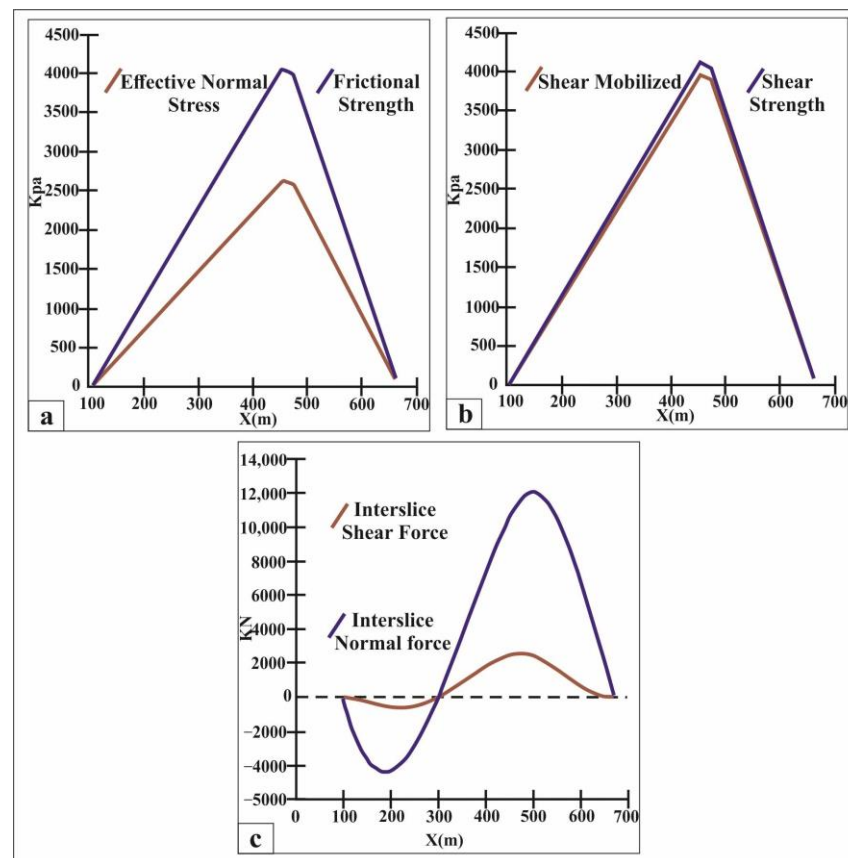


**Figure 9.** Strength parameters of Case—01 for Miacher Slope, (a) Effective Normal Stress vs Frictional Strength acting on Miacher slope, (b) Shear Mobilized vs Shear Strength of Miacher Slope, (c) Interslice Shear force vs Interslice Normal force acting on Miacher Slope.

#### Case Two: Thickness 200 m and wet conditions

An assumption was made to represent the slope condition as wet, GWT was raised by 100 m and overburden remained constant (200 m) due to the development of PWP. The phreatic level correction in Slope/w was taken into account by the presence of a water table and the pore water pressure distribution was calculated accordingly. The FOS simulated via different methods is shown in Figure 8b.

From Figure 10a, the peak values of frictional strength and effective normal stress were 4000 kPa and 2500 kPa with an increase in frictional strength by an amount of 1500 kPa, reinforcing the stability. The shear strength surpassed the shear mobilized by an amount of 500 kPa (Figure 10b). The peak value of interslice normal force was 10,000 kN with interslice shear force reaching 2500 kN, with a total change of 7500 kN augmenting the

stability by that amount (Figure 10c). At a groundwater level of 100 m, the Miacher slope is stable, as the strength parameters are greater than the stress parameters. The effect of Pore Water Pressure (PWP) is negligible as it is negative, thereby enhancing the stability (Figure 10d).

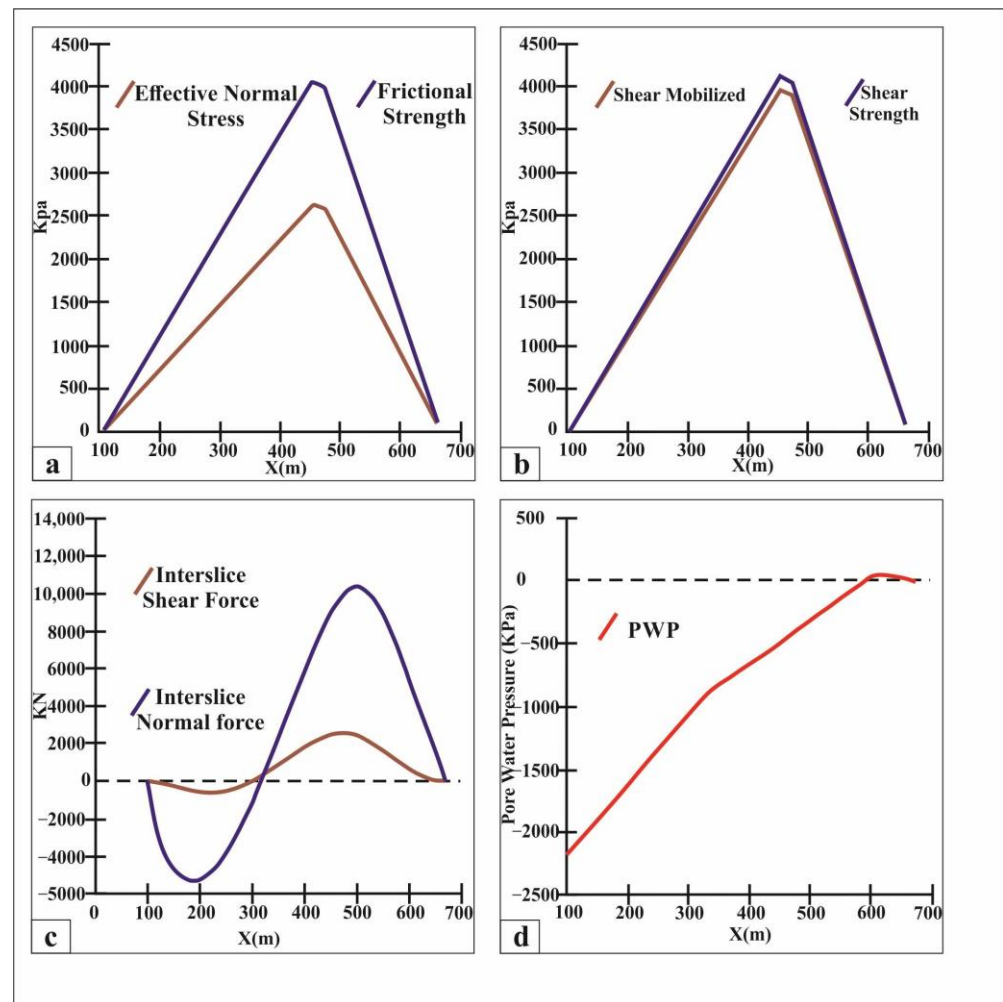


**Figure 10.** Strength parameters of Case 2 for Miacher Slope, (a) Effective Normal Stress vs Frictional Strength acting on Miacher slope, (b) Shear Mobilized vs Shear Strength of Miacher Slope, (c) Interslice Shear force vs Interslice Normal force acting on Miacher Slope, (d) Pore Water Pressure (PWP) along the Miacher Slope with increase of ground water level during wet season.

The FOS for Cases one and two (Figure 8a,b) was almost the same as that for Morgenstern and Price and Ordinary methods; the Janbu method showed a decrease in FOS by a factor of 6% with respect to Case one, and the Bishop method showed an increase in FOS by an amount of 2% with respect to Case one. All these analyses showed that as the groundwater table (GWT) rises to a certain level, it increases the pore water pressure (PWP) in the soil and reduces the effective stress, which can enhance the slope stability. However, if the GWT continues to rise, the excess water can cause soil particles to become suspended and reduce inter-soil adhesive and cohesive forces, which can decrease the FOS and increase the likelihood of slope failure. Therefore, there is a threshold beyond which the rise in GWT becomes detrimental to slope stability.

#### Case Three: Thickness 100 m and dry conditions

In Case three, the thickness of the overburden was decreased to 100 m, while keeping the condition dry showed a progressive result on the stability and FOS (Figure 8c). It is evident after analysis that both MP and Ordinary methods showed an increase of 2%

and 1.8% in FOS relative to Cases one and two, respectively. FOS in the Janbu method showed a decrease of 3.5% with respect to Case one and an increase of 1.85% with respect to Case two. In the case of the Bishop method, an increase of 3.2% in FOS relative to Case one and 1.8% relative to Case two was recorded. The strength parameter of frictional strength and shear strength had a peak value of 2800 kPa and 2900 kPa, while destabilizing parameters effective normal stress peaked at 1800 kPa and that of shear mobilized at 2700 kPa (Figure 11a,b). The interslice normal force reached a peak value of 10,200 KN, responsible for the enhanced FOS with respect to Cases one and two (Figure 11c). From the analysis of Case three, it is concluded that a decrease in the overburden of the materials increases the strength properties of the soil and, hence, the FOS.

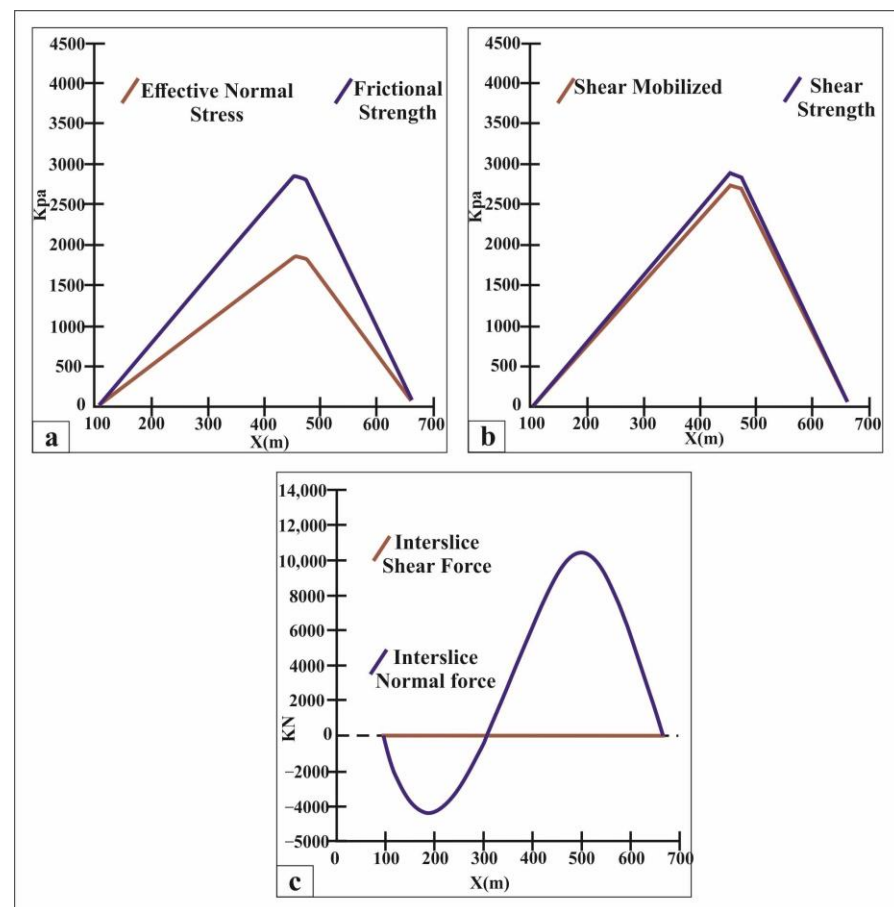


**Figure 11.** Strength parameters of Case 3 for Miacher Slope. (a) Effective Normal Stress vs Frictional Strength acting on Miacher slope, (b) Shear Mobilized vs Shear Strength of Miacher Slope, (c) Interslice Shear force vs Interslice Normal force acting on Miacher Slope.

#### Case Four: Thickness 100 m and wet conditions

In this case, at a thickness of 100 m with wet conditions, the PWP was developed while keeping the thickness of overlying materials constant (Figure 8d). It was observed that the FOS decreased by 1% with respect to Case three and increased by an amount of 1% with respect to Cases one and two. Similarly, the Ordinary method showed a 1.4% decrease in FOS from Case two and increased by an amount of 0.3% with respect to Case three. The Janbu method showed a decrease of 1.4 and 5.0% in FOS with respect to Case three and Case one, respectively, and an increase of 0.3% with respect to Case two. The B method showed no change in FOS with respect to Case three, and an increase of 1.7% and 3.2% in FOS with respect to cases two and one, respectively.

The graphs regarding the effective normal stress and the frictional strength were plotted with peak frictional strength and normal stress values of 3700 and 2300 Kpa,

respectively (Figure 12a). The frictional strength aided slope stability by an amount of 1400 Kpa. The shear strength had a maximum value of 3800 kPa, while that of the shear mobilized reached a maximum value of 3700 Kpa, thereby making a total difference of 100 kPa, which aided the stability of the Miacher slope (Figure 12b). The Interslice normal force attained its maximum value of 47,000 KN, aiding slope stability (Figure 12c). The PWP became negative at the start of the slope, while it became positive when the slope distance increased the PWP and reached a peak value of 200 Kpa responding to different stability parameters and disrupting the slope by an amount of 1 to 2% with respect to Case three (Figure 12d).

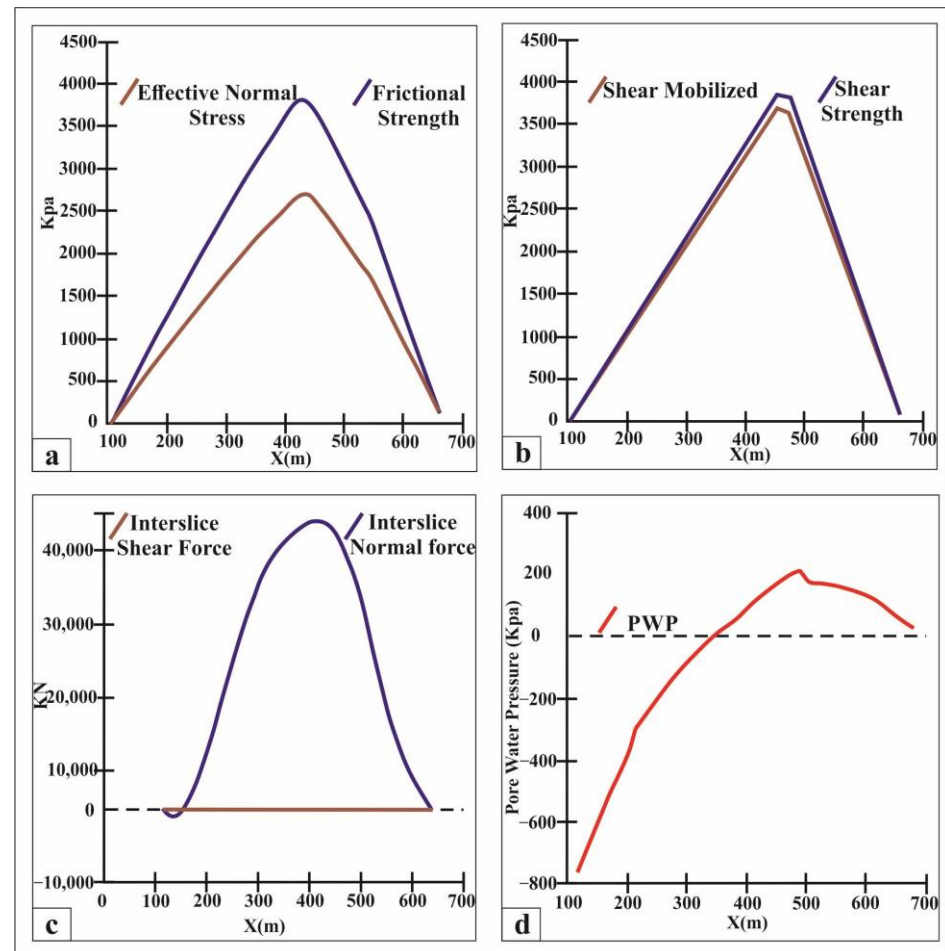


**Figure 12.** Strength parameters of Case 4 for Miacher Slope, (a) Effective Normal Stress vs Frictional Strength acting on Miacher slope, (b) Shear Mobilized vs Shear Strength of Miacher Slope, (c) Interslice Shear force vs Interslice Normal force acting on Miacher Slope, (d) Pore Water Pressure (PWP) along the Miacher Slope with increase of ground water level during wet season.

It is inferred from Case four that the increase in PWP tends to destabilize the slope by decreasing the FOS in the Miacher slope. The PWP is either increased in a natural way or anthropogenically and should be controlled by proper management. In the Miacher slope, the natural ways include rainfall, while anthropogenic activities are the sewerage water, septic tanks and flooding of the fields as water continuously pours through the loose materials and, hence, destabilizes the slope. Proper management of water resources, including the control of water discharge from anthropogenic sources, can help reduce the risk of slope failure due to an increase in PWP. In addition, appropriate slope stabilization measures, such as the construction of retaining walls and soil nailing, can also be implemented to improve slope stability. It is important to regularly monitor the slope and take

appropriate measures in case of any signs of instability or failure to ensure the safety of the surrounding community.

#### Case Five: FOS via probability and dry conditions

Assuming that the soil unit weight changes as a result of the weathering of metamorphic rock at a different pace, the probability of the Miacher slope was estimated employing three different unit weights, 11, 12 and 13. The Miacher slope's probabilistic analysis was modeled using predetermined values. As stated in Figure 7e, the slope was stable with an FOS of 1.036 and a reliability index of 5.403, indicating that the slope is secure in the present settings. There was a lower likelihood of failure, as indicated by the frequency via FOS and probability density function chart (Figure 13a,b).

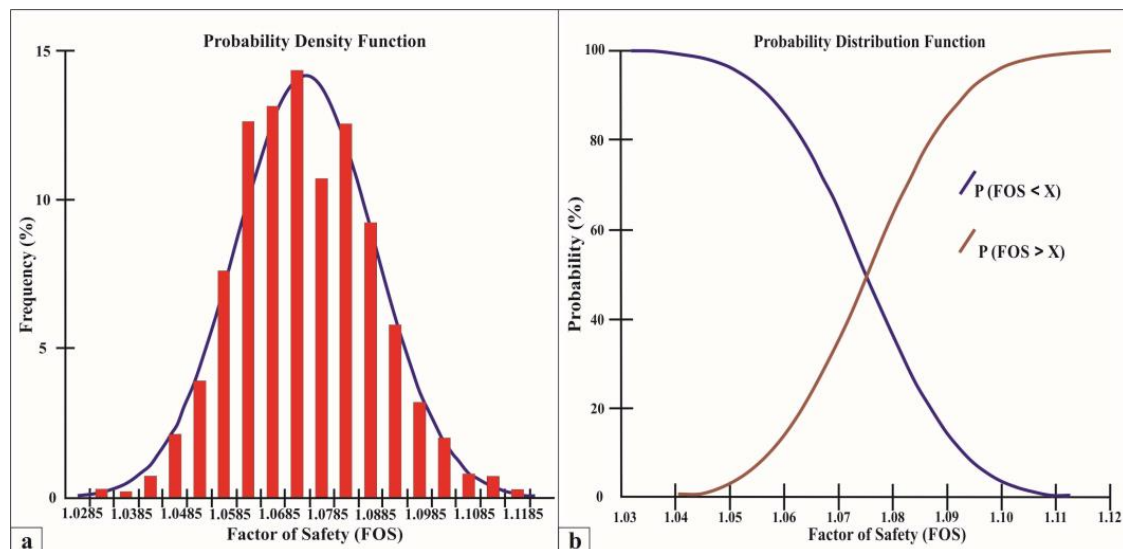


**Figure 13.** Probabilistic analysis of Miacher slope in dry season, Case 5, (a) FOS distribution along the Miacher Slope, (b) FOS distribution along the Miacher Slope along X and Y direction.

#### Case Six: FOS via probability and wet season

In order to determine the impacts of the three distinct unit weights (11, 12 and 13) on slope stability, the probability function for the wet season was generated and its implications on slope stability were examined. With  $FOS = 0.866$ , the study of the current conditions using Slope/w revealed that the slope was unstable (Figure 8f). The slope's reliability index was  $-5.748$ , which means it was insecure under the circumstances (Figure 8f). The research shows that a small modification to the PWP would significantly impact the FOS. In comparison with the case in point five, the FOS for the MP technique changed by 16%, while the FOS for the O and J methods changed by 12 and 15%, respectively. The analysis suggests that altering the soil characteristics and PWP conditions has a significant impact on slope stability. To prevent failure in the case of the Miacher slope, the pore water needs to be managed. Due to increases in the PWP, the probability density and distribution functions indicated a significant probability of failure (Figure 14a,b).

#### Case Seven: Sensitivity of the slope under dry conditions

With the input of various stability factors, the sensitivity analysis was carried out using Slope/w to calculate FOS. Different strength characteristics were used in the sensitivity study, including unit weight, cohesiveness and angle of internal friction. Sensitivity analysis was used to assess the impact of various stability parameters on both stability and FOS. By subtracting the standard deviations for unit weight, internal friction angle and cohesiveness, the sensitivity analysis's standard deviation was calculated.

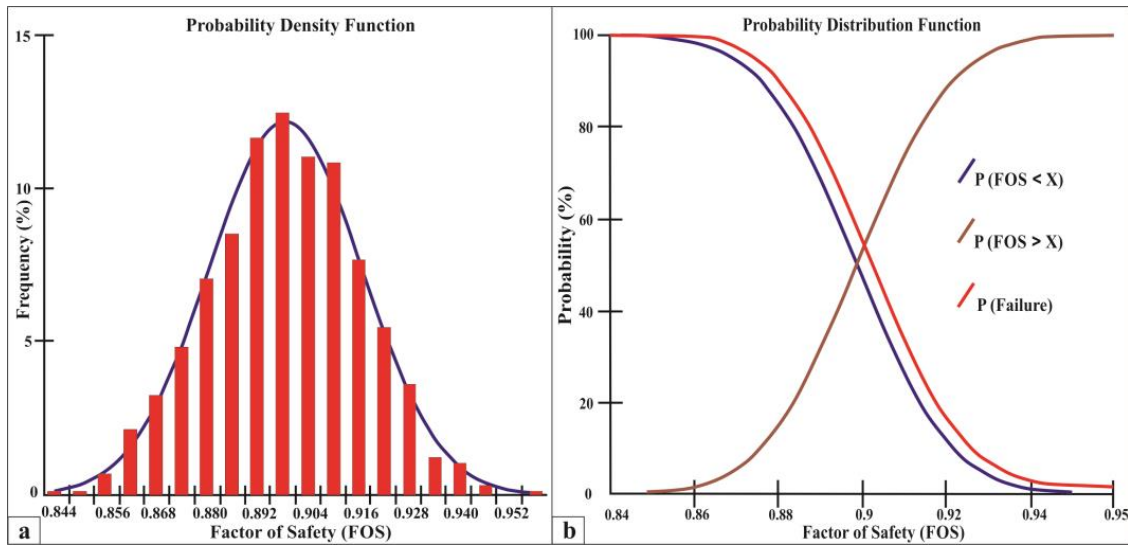


**Figure 14.** Probabilistic analysis of Miacher slope in wet season, Case 6, (a) FOS distribution along the Miacher Slope, (b) FOS distribution along the Miacher Slope along X and Y direction and failure curve from crest to the toe of Miacher Slope.

For a dry slope without PWP development or one that is very deep, the FOS was calculated (Figure 8g). The sensitivity chart for various strength settings is displayed in (Figure 15). The FOS distribution for unit weight, cohesion and angle of internal friction using the sensitivity analysis is shown in Table 4. The graph makes it obvious that the FOS and sensitivity have a direct linear relationship for both unit weight and cohesiveness. Figure 15 shows that the FOS and cohesion have the same linear relationship, with a change in unit weight of one, changing the FOS by 0.5%, and a change in cohesion by a factor of standard deviation 10, changing the FOS by 0.5%. A number of two for the angle of internal friction would result in a 10% change in FOS. FOS and slope stability would both rise as the angle of internal friction increased.

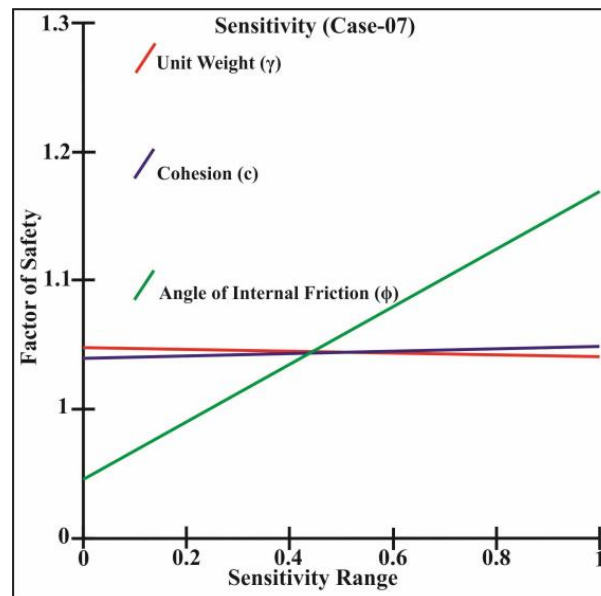


**Figure 15.** Sensitivity analysis of Miacher slope in dry season Case 7.

**Table 4.** Showing Sensitivity for Case seven’s different methods with different unit Weight, Angle of Internal Friction and Cohesion.

Parameters	Factor of Safety (FOS)								
	Unit Weight ( $\gamma$ )			Cohesion (C)			Angle of Internal Friction ( $\Phi$ )		
	11	12	13	50	60	70	26	28	30
MP	1.046	1.036	1.026	1.026	1.031	1.036	1.016	1.036	1.056
O	1.032	1.028	1.024	1.020	1.024	1.028	1.010	1.028	1.046
J	1.032	1.028	1.024	1.020	1.024	1.028	1.010	1.028	1.046
B	1.048	1.044	1.041	1.039	1.041	1.044	0.944	1.044	1.168

MP = Morgenstern & Price, O = Ordinary, J = Janbu, B = Bishop

**Case Eight: Sensitivity of the slope in the wet season**

With the exception of the PWP being altered and the consequences on the slope stability being calculated, this scenario was comparable to that of Case seven (Figure 16). The analysis shows that a small change in the PWP causes a small change in the FOS. Compared with scenario seven, the FOS of the MP approach changed by 1%. In a similar way, the O, J and B methods differ from (Figure 8h) by 1%. It is clear from the research that there would be little impact on FOS with a small change in the soil’s qualities, such as unit weight, friction and cohesiveness, in the case of PWP. The sensitivity chart (Table 5) demonstrates that the angle of internal friction, which must be taken into account when doing a stability analysis, is crucial. According to the analysis, in order to stabilize the slope, the angle of internal friction should be increased through either suitable drainage pipe installation or cementing.

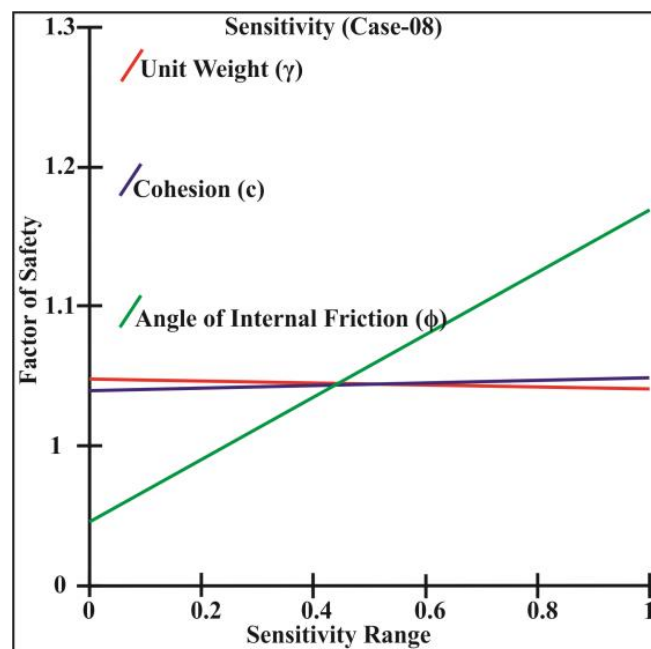


**Figure 16.** Sensitivity analysis of Miacher slope in wet season, Case 8.

**Table 5.** Showing Sensitivity for Case seven's different methods with different unit Weight, Angle of Internal Friction and Cohesion.

FOS														
$\gamma$	MP	O	J	B	$\phi$	MP	O	J	B	c	MP	O	J	B
<b>11</b>	1.053	1.020	1.020	1.045	<b>26</b>	1.023	1.015	1.015	0.942	<b>50</b>	1.024	1.018	1.018	1.036
<b>12</b>	1.033	1.025	1.025	1.042	<b>28</b>	1.033	1.025	1.025	1.042	<b>60</b>	1.028	1.021	1.021	1.039
<b>13</b>	10.13	1.030	1.030	1.038	<b>30</b>	1.043	1.035	1.035	1.165	<b>70</b>	1.033	1.025	1.025	1.042

( $\gamma$  = Unit weight KN/m<sup>3</sup>,  $\phi$  = Angle of Internal friction, c = Cohesion)  
MP = Morgenstern & Price, O = Ordinary, J = Janbu, B = Bishop

#### 4. Geochemistry and Geological Analysis

##### 4.1. Effect of Mineralogy

The type of cementing material, clay minerals and other main or secondary minerals were identified using XRD analysis, which was carried out in the NCEG XRD lab in Peshawar's University. Powdered samples were briefly put through an XRD apparatus (Rigaku Radiation Shield). The tube current was set at 20 mA and the voltage was set to 35 kV. Step size was set at 0.05, step time to 1 s, destination angle to 65 and start angle to 2. The wavelength was 1.5405 and the intensity scale was set to 2000. The Rigaku Radiation Shield's default software, XS 2007 XRD measurement, was used for the process, and Origin was used to produce the data. The Standard X-ray Diffraction Powder Patterns' XRD mineral databases were used to analyze the XRD charts [62]. Additionally, web mineral data and Mindat were used as online databases.

##### 4.2. Mineralogy

The analysis of soil samples (n = seven) via XRD showed that quartz, clay and feldspar were among the main minerals with small proportions of plagioclase, calcite and dolomite minerals (Figure 17). The clay minerals found in the soil samples were mostly illite, kaolinite and muscovite, which were mostly formed by the disintegration of metasedimentary rocks. Quartz and calcite were acting as the cementing materials enhancing the stability of the soil, as quartz is most resistant to weathering and disintegration. Feldspar and plagioclase are more susceptible to weathering and are easily converted to clay. During XRD analysis, no swelling clays such as smectite and montmorillonite were detected.

##### 4.3. Effect of Geology on the Miacher Slope

In the Main Karakoram Thrust (MKT) Zone, the Miacher hamlet is situated where the Kohistan Island Arc and the Eurasian Block converge (Figure 2). The geomorphology of the studied area showed that the landforms were formed in a glaciofluvial valley that the Hunza River carved out, and that glacial moraines are still visible on the valley's side slopes (Figure 18). The following geomorphologic units, ranging in altitude from low to high and affecting the stability of the slope, are found in the region of Miacher village.

###### 4.3.1. Hunza River

With a catchment area of roughly 4463 km<sup>2</sup>, the Hunza River basin has a surface area of 13,733 km<sup>2</sup> and is located in the hilly terrain of central Karakoram at a high height of over 5000 m. The Hunza River flows at the bottom of a slope that is 10 m wide when velocity is at its highest. The Hunza River's mean annual flow is 323 m<sup>3</sup> s<sup>-1</sup>, with summer being the peak because of precipitation and glacial melt and winter being the lowest. The Hunza River erodes the slope's toe, especially in the summer when the flood plain is completely covered and subject to sliding due to high velocity and flow.

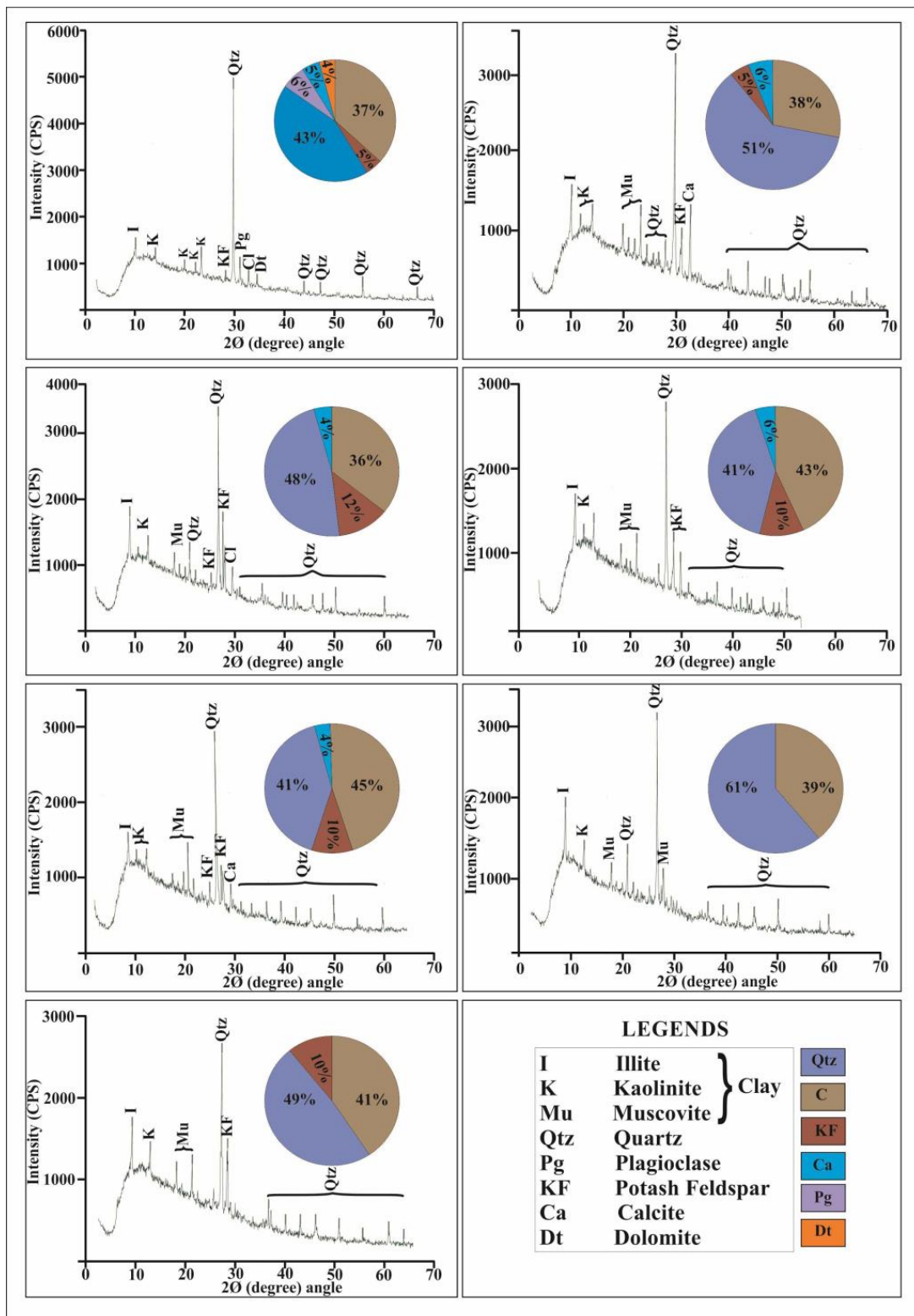
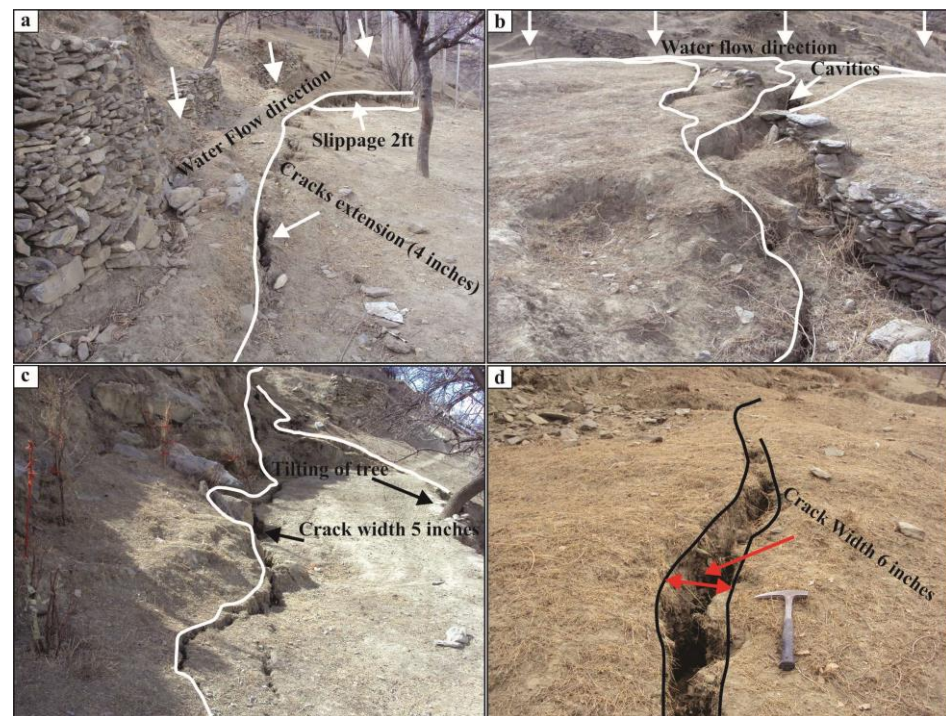


Figure 17. XRD analysis of Miacher soil for its geochemical composition.



**Figure 18.** Different types of cracks (a–d) in Miacher soil.

#### 4.3.2. Anthropogenic/Agricultural Activities

The term “anthropogenic activities” refers to household and agricultural operations. The slope’s unit weight and PWP are continuously increased by the irrigation system’s unplanned addition of water. There is no channel for the transportation of irrigation water in agriculture. Additionally, there is no adequate sewer system; instead, water gets infiltrated from other sources as well as the septic and soakage tanks. Two hundred dwellings make up the Miacher town; if each one uses a gallon of water per day, 200 gallons per day would be added to the slope.

#### 4.3.3. Cracks

Both the soil and the rocks of the Miacher slope, which differ in their geology, dynamics and history, have well-developed cracks. In the research area’s fissures are either tensional or gravitational cracks, both of which affect stability. These fissures, which are disconnected from the primary soil mass, are caused by the soil losing the ability to maintain stability. Along the slope’s length and width, the cracks are well-developed. The fissures range in length from 10 to 20 m and in diameter from 5 to 15 inches.

Figure 18a demonstrates that the crack’s breadth and extension are both about 4 inches, and the amount of block slippage is about 2 feet. Additionally, the direction of the water flow through the fissures and instability is depicted. The collapse of the soil depicted in Figure 18b led to the development of the daughter cracks, as well. Figure 18c shows that the tree is tilting, indicating that movement is still occurring; the break in this image is 5 inches wide. Due to the collapse of soil strength, the crack’s breadth fluctuates and can be as wide as 6 inches (Figure 18d). The tensional break where one block slipped in relation to the other is depicted in Figure 19a. According to discussions with local Miacher village residents, the slippage began in 2010 and was approximately 4 feet. However, in June 2013, following irrigation, the movement restarted, and the block went down and reached 10 feet, as measured in February 2014. The wooden nails that have been put to track ground movement are shown in Figure 19b. A total of 2014 measurements show that one block shifted away from the other by around 2 feet.

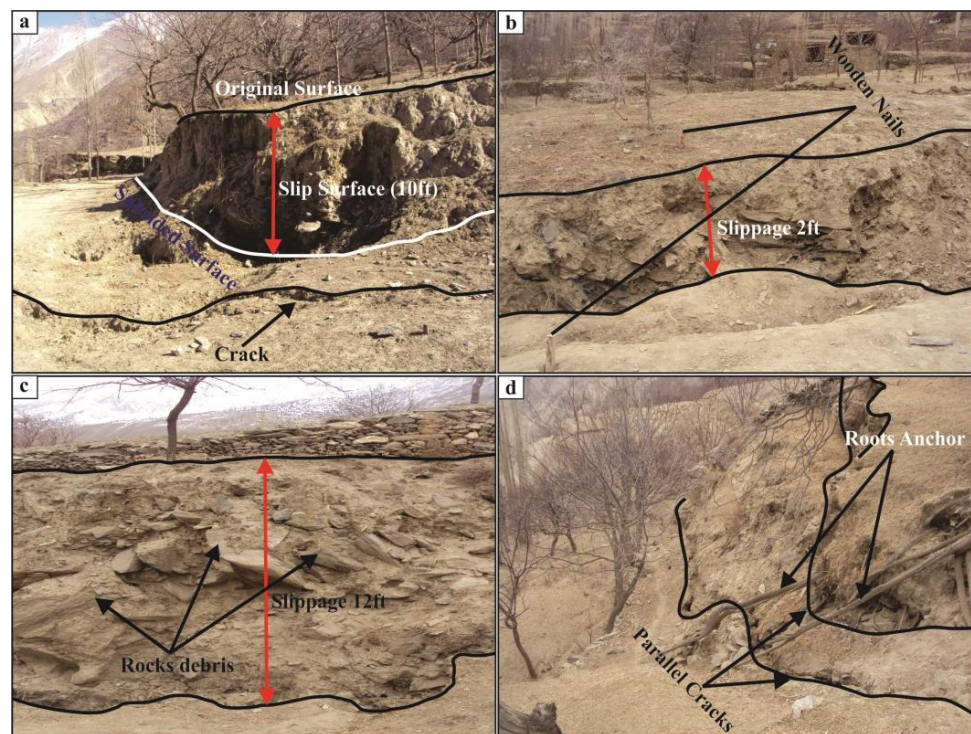


Figure 19. Different types of cracks (a–d) in Miacher soil.

Additionally, Figure 19c demonstrates the 12-foot slippage. The two blocks were in the same location in 1980 when the field was being used for irrigation, but after that, the movement started gradually, and in a period of 34 years, the slippage reached 12 feet, according to a senior member of the village. At the slope’s head and running its whole length, a series of parallel fissures appeared, as shown in Figure 19d. Along the entire slope, these parallel fissures were regularly evident.

#### 4.3.4. Shear Zones

Along the slope where rocks have been crushed and sheared by tectonic and compressional pressures, a well-developed shear zone is evident in the NE–SW direction. Along these zones, the rocks were fragmented, weaker and less coherent, making them more likely to fail when subjected to gravity (Figure 20a).

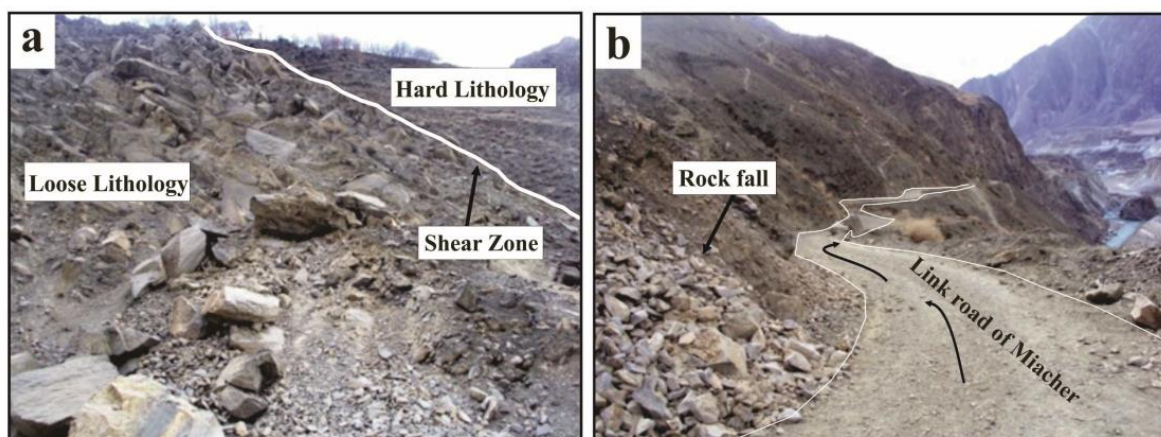


Figure 20. (a) Shear zone observed at Miacher Hunza; (b) link road of Miacher and Minapin Hunza.

#### 4.3.5. Construction of Road

The construction of a road along this path has been attempted to connect Miacher village to the Karakoram Highway via Minapin village (Figure 20b). However, as work on the road progressed, Miacher village residents noticed the slope shifting and cracks appearing. Due to the reduction in slope angle at the slope's base and the ground shaking caused by the use of heavy machinery during the construction of the road, the movement was caused by the road's construction.

#### 4.4. Effect of Precipitation on Slope Stability

The primary input to the hydrological cycle is precipitation, which contributes either directly as rain or indirectly as snow. It is a major cause of mass movement because of mechanical weathering, freeze–thaw action, the conveyance of debris flows and because it acts as a lubricant for mass movement, including slipping and sliding mechanisms.

Precipitation causes the slide in a number of ways, such as that rainfall alters GWT and that variations in water level may lead to PWP changes in shoreline soil slopes. Additionally, this modification might be crucial to lowering FOS. As a result, it is highly helpful to accurately determine PWP or phreatic line in the waterfront slopes in order to examine the stability of the slopes. The problem has been the subject of some important works, according to [5,7,44,63]. In essence, seepage and frequent pore pressure changes degrade the sediment effectively, allowing it to be ruled out for the area that is now stable.

The current analysis used rainfall trends from 2007 to 2022 to illustrate the likely impact of precipitation on the Miacher slope. The Pakistan Meteorological Department (PMD) of Hunza Station provided the rainfall information for this time period. For each of the three seasons, monsoon, pre-monsoon and post-monsoon, the rainfall trend was examined (Figure 20).

##### 4.4.1. Monsoon

The monsoon season, which spans the four months of June through September, has a precipitation tendency that can be seen. According to the analysis, the month of July 2007 had the most rainfall with 244 mm, followed by September with 211 mm, June with 151 mm and August with 119 mm. Again, in 2010 and 2011, the months of July and September saw the highest amounts of rainfall (68 and 65 mm, respectively) (Figure 21a). Between 2007 and 2022, the highest amounts of rainfall recorded in the months of July and September were 421 and 385 mm, respectively. The measured annual trend reveals a recurrent pattern with high and low rainfall intensity over a period of seven years. The highest precipitation occurred in June and July, which is predicted to have a negative impact on sliding based on the analysis of the monthly trend in the monsoon [63,64].

##### 4.4.2. Pre-Monsoon

For the months of February to May, the pre-monsoon rainfall trend was examined. It was noted that the highest amounts of precipitation—188 and 46 mm, respectively—were recorded in April 2008 and 2012 (Figure 21b). The maximum amounts of rainfall in May 2008 and 2010 were 80 and 52 mm, respectively. From 2007 to 2013, the maximum precipitation was recorded in May and April, with 342 and 233 mm, respectively, according to the yearly pattern for the pre-monsoon (Figure 20). The two-year timeframe of the observed year-by-year pattern likewise reveals a periodic trend with high and low rainfall intensity [65].

##### 4.4.3. Post-Monsoon

For the months of October through January, the post-monsoon rainfall trend was examined. It was noted that the month of January in the year 2009 had the highest rainfall total, which was 24 mm. From 2007 to 2022, the highest amounts of rainfall recorded in the months of October and January were 48 mm and 40 mm, respectively (Figure 21c). The two-year trend in rainfall intensity is shown to follow a cyclical pattern with high and low rainfall intensity [65].

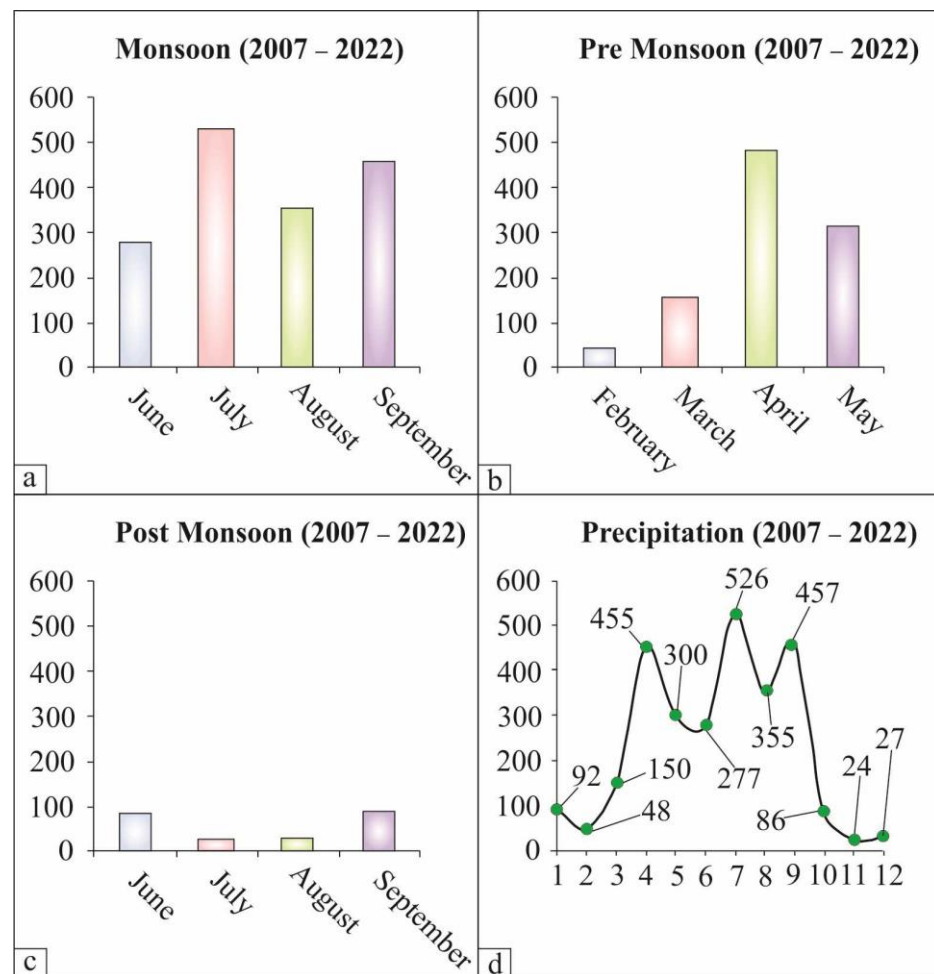


**Figure 21.** Rainfall trend analysis: (a) monsoon; (b) pre-monsoon; (c) post-monsoon; (d) precipitation from 2007 to 2022.

#### 4.4.4. Interpretation

A correlation between pore water pressure and landslide displacement, rainfall and pore water pressure and rainfall and landslide displacement can be inferred from fifteen years of rainfall data in the Hunza region (Figure 21d). This suggests that consistent and protracted rainfall can affect pore water pressure more than brief but severe downpours [43]; intense rainfall episodes may also trigger shallow landslides. When severe rainfall lasts for an extended length of time, the likelihood of massive landslides increases [9,43,64–66]. The stability is significantly impacted by the months of July, September and April. It can be concluded that there is a substantial likelihood that a landslide will occur during these months. Rain acts as a lubricant by decreasing the inter-granular strength (adhesive and cohesive) while also raising the pore water pressure. A suitable piezometer or stand pipe should be constructed to record the pore water pressure in order to evaluate the rise in pore water pressure throughout these months [65]. Additionally, historical landslide data must be preserved in order to determine how frequently landslides occur during certain months of the year.

## 5. Conclusions

According to Slope/w's simulation of the current conditions, the Miacher slope is geotechnically only partially stable; the FOS regarding all methods was higher than one. The FOS was linearly increased proportionally as the cohesiveness and the angle of the internal friction were increased [65]. Additionally, the increase in values in unit weight and overburden of overlying material negatively affected FOS. According to the cracks seen

in the Miacher soil, there is still movement occurring on the Miacher slope. Progressive or partial slope failure is more probable than complete slope failure [65]. Outcrops in the sliding region seem to prevent complete slope failure. According to the aforementioned conclusions, the following suggestions are advised:

- Each and every manmade alteration as well as natural element substantially accelerates slope collapse. In this regard, the creation of a concrete channel should be used to manage the infiltration of sewage, irrigation and surface runoff water into the gaps and caves.
- Existing fractures should be filled and sealed with regional material, ideally impermeable clay, to improve the soil's cohesiveness.
- Avoid base cutting on the grounds that it will reduce the slope angle and have a detrimental impact on the FOS.
- A detailed Geophysical survey including gravity, resistivity and GPR should be conducted to picture the 2D model of the landslide assisted by the installation of a GNSS receiver, particularly in the rainy season, to capture the rate of movement of incipient landslide.

**Author Contributions:** Conceptualization, M.u.R. and W.A.; methodology, M.u.R., W.A. and I.I.; software, M.u.R., W.A. and I.I.; validation, M.u.R., I.I. and W.A.; formal analysis, M.u.R. and W.A.; investigation, M.u.R., W.A. and I.I.; resources, W.A. and I.I.; data curation, M.u.R.; writing—original draft preparation, M.u.R.; writing—review and editing, M.u.R., I.I., P.P., P.P.G. and N.K.; visualization, P.P., P.P.G., N.K. and I.I.; supervision, W.A.; project administration, W.A. and I.I.; funding acquisition, P.P., P.P.G. and N.K. All authors have read and agreed to the published version of the manuscript.

**Funding:** This research received no external funding.

**Data Availability Statement:** The authors will provide the data associated with this manuscript, without restriction, to readers and researchers elsewhere working on related research based upon reasonable request.

**Acknowledgments:** This is to acknowledge that this manuscript is part of first author Mehboob Ur Rashid's M.S. thesis/dissertation work submitted to the University of Peshawar. We would like to thank the National Centre of Excellence in Geology, University of Peshawar for providing resources for this study. The authors are highly indebted to Pakistan Meteorological Organization for providing rainfall data to carry out this research work.

**Conflicts of Interest:** The authors declare no conflict of interest.

## References

1. Zou, Q.; Jiang, H.; Cui, P.; Zhou, B.; Jiang, Y.; Qin, M.; Liu, Y.; Li, C. A new approach to assess landslide susceptibility based on slope failure mechanisms. *Catena* **2021**, *204*, 105388. [[CrossRef](#)]
2. Crozier, M.J.; Glade, T. Landslide hazard and risk: Issues, concepts and approach. *Landslide Hazard Risk* **2005**, 1–40. [[CrossRef](#)]
3. Kundu, P.; Gupta, N. Impact of residual strength of soil in reactivated landslide: Case studies of a few landslides in different regions of the globe. In *Earthquake Geotechnics: Select Proceedings of 7th ICRAGEE 2021*; Springer: Singapore, 2022; pp. 249–258.
4. Reale, C.; Gavin, K.; Prendergast, L.J.; Xue, J. Multi-modal reliability analysis of slope stability. *Transp. Res. Procedia* **2016**, *14*, 2468–2476. [[CrossRef](#)]
5. Chirico, G.B.; Borga, M.; Tarolli, P.; Rigon, R.; Preti, F. Role of vegetation on slope stability under transient unsaturated conditions. *Procedia Earth Planet. Sci.* **2013**, *19*, 932–941. [[CrossRef](#)]
6. Sur, C.; Jung, Y.; Choi, M. Temporal stability and variability of field scale soil moisture on mountainous hillslopes in Northeast Asia. *Geoderma* **2013**, *207–208*, 234–243. [[CrossRef](#)]
7. Sorbino, G.; Nicotera, M.V. Unsaturated soil mechanics in rainfall-induced flow landslides. *Eng. Geol.* **2013**, *165*, 105–132. [[CrossRef](#)]
8. L'Heureux, J.S.; Vanneste, M.; Rise, L.; Brendryen, J.; Forsberg, C.F.; Nadim, F.; Longva, O.; Chand, S.; Kvalstad, T.J.; Haflidason, H. Stability, mobility and failure mechanism for landslides at the upper continental slope off Vesterålen, Norway. *Mar. Geol.* **2013**, *346*, 192–207. [[CrossRef](#)]
9. Kanungo, D.P.; Sharma, S. Rainfall thresholds for prediction of shallow landslides around Chamoli-Joshimath region, Garhwal Himalayas, India. *Landslides* **2013**, *11*, 629–638. [[CrossRef](#)]
10. McKenna, J.; Santi, P.; Amblard, X.; Negri, J. Effects of soil-engineering properties on the failure mode of shallow landslides. *Landslides* **2012**, *9*, 215–228. [[CrossRef](#)]

11. Ho, J.-Y.; Lee, K.T.; Chang, T.-C.; Wang, Z.-Y.; Liao, Y.-H. Influences of spatial distribution of soil thickness on shallow landslide prediction. *Eng. Geol.* **2012**, *124*, 38–46. [[CrossRef](#)]
12. Butt, M.J.; Umar, M.; Qamar, R. Landslide dam and subsequent dam-break flood estimation using HEC-RAS model in Northern Pakistan. *Nat. Hazards* **2013**, *65*, 241–254. [[CrossRef](#)]
13. Afzal, N.; Ahmad, A.; Shirazi, S.A.; Younes, I. GIS-based landslide susceptibility mapping using analytical hierarchy process: A case study of Astore region, Pakistan. *EQA-Int. J. Environ. Qual.* **2022**, *48*, 27–40. [[CrossRef](#)]
14. Hussain, M.A.; Chen, Z.; Wang, R.; Shah, S.U.; Shoaib, M.; Ali, N.; Xu, D.; Ma, C. Landslide susceptibility mapping using machine learning algorithm. *Civ. Eng. J.* **2022**, *8*, 209–224. [[CrossRef](#)]
15. Khaliq, A.H.; Basharat, M.; Riaz, M.T.; Riaz, M.T.; Wani, S.; Al-Ansari, N.; Le, L.B.; Linh, N.T.T. Spatiotemporal landslide susceptibility mapping using machine learning models: A case study from district Hattian Bala, NW Himalaya, Pakistan. *Ain Shams Eng. J.* **2023**, *14*, 101907. [[CrossRef](#)]
16. Kamp, U.; Growley, B.; Khattak, G.; Owen, L. GIS-based landslide susceptibility mapping for the 2005 Kashmir earthquake region. *Geomorphology* **2008**, *101*, 631–642. [[CrossRef](#)]
17. Ullah, I.; Aslam, B.; Shah, S.H.I.A.; Tariq, A.; Qin, S.; Majeed, M.; Havenith, H.-B. An integrated approach of machine learning, remote sensing, and GIS data for the landslide susceptibility mapping. *Land* **2022**, *11*, 1265. [[CrossRef](#)]
18. Farooq, S.; Akram, M.S. Landslide susceptibility mapping using information value method in Jhelum Valley of the Himalayas. *Arab. J. Geosci.* **2021**, *14*, 824. [[CrossRef](#)]
19. Khalil, U.; Imtiaz, I.; Aslam, B.; Ullah, I.; Tariq, A.; Qin, S. Comparative analysis of machine learning and multi-criteria decision making techniques for landslide susceptibility mapping of Muzaffarabad district. *Front. Environ. Sci.* **2022**, *10*, 1028373. [[CrossRef](#)]
20. Khan, A.N.; Collins, A.E.; Qazi, F. Causes and extent of environmental impacts of landslide hazard in the Himalayan region: A case study of Murree, Pakistan. *Nat. Hazards* **2011**, *57*, 413–434. [[CrossRef](#)]
21. Qasim, S.; Qasim, M.; Shrestha, R.P. A survey on households' resilience to landslide hazard in Murree hills of Pakistan. *Environ. Chall.* **2021**, *4*, 100202. [[CrossRef](#)]
22. Amin, M.N.; Umair Ashfaq, M.; Mujtaba, H.; Ehsan, S.; Khan, K.; Faraz, M.I. Computer-Aided Slope Stability Analysis of a Landslide—A Case Study of Jhika Gali Landslide in Pakistan. *Sustainability* **2022**, *14*, 12954. [[CrossRef](#)]
23. Qasim, S.; Qasim, M.; Shrestha, R.P.; Khan, A.N. Socioeconomic determinants of landslide risk perception in Murree hills of Pakistan. *Aims Environ. Sci.* **2018**, *5*, 305–314. [[CrossRef](#)]
24. Feng, H.; Lu, H.; Carrapa, B.; Zhang, H.; Chen, J.; Wang, Y.; Clift, P.D. Erosion of the Himalaya-Karakoram recorded by Indus Fan deposits since the Oligocene. *Geology* **2021**, *49*, 1126–1131. [[CrossRef](#)]
25. Clift, P.D.; Shimizu, N.; Layne, G.; Blusztajn, J.; Gaedicke, C.; Schluter, H.-U.; Clark, M.; Amjad, S. Development of the Indus Fan and its significance for the erosional history of the Western Himalaya and Karakoram. *Geol. Soc. Am. Bull.* **2001**, *113*, 1039–1051. [[CrossRef](#)]
26. Su, X.; Zhang, Y.; Meng, X.; Rehman, M.U.; Khalid, Z.; Yue, D. Updating Inventory, Deformation, and Development Characteristics of Landslides in Hunza Valley, NW Karakoram, Pakistan by SBAS-InSAR. *Remote Sens.* **2022**, *14*, 4907. [[CrossRef](#)]
27. Rehman, Q.U.; Ahmed, W.; Waseem, M.; Khan, S.; Farid, A.; Shah, S.H.A. Geophysical investigations of a potential landslide area in Mayoan, Hunza District, Gilgit-Baltistan, Pakistan. *Rud. -Geološko-Naft. Zb.* **2021**, *36*, 127–141. [[CrossRef](#)]
28. Rehman, M.U.; Zhang, Y.; Meng, X.; Su, X.; Catani, F.; Rehman, G.; Yue, D.; Khalid, Z.; Ahmad, S.; Ahmad, I. Analysis of landslide movements using interferometric synthetic aperture radar: A case study in Hunza-Nagar Valley, Pakistan. *Remote Sens.* **2020**, *12*, 2054. [[CrossRef](#)]
29. Ahmed, M.F.; Ali, M.Z.; Rogers, J.D.; Khan, M.S. A study of knickpoint surveys and their likely association with landslides along the Hunza River longitudinal profile. *Environ. Earth Sci.* **2019**, *78*, 176. [[CrossRef](#)]
30. Bacha, A.S.; Shafique, M.; van der Werff, H. Landslide inventory and susceptibility modelling using geospatial tools, in Hunza-Nagar valley, northern Pakistan. *J. Mt. Sci.* **2018**, *15*, 1354–1370. [[CrossRef](#)]
31. Ahmed, M.F.; Rogers, J.D.; Bakar, M.Z.A. Hunza river watershed landslide and related features inventory mapping. *Environ. Earth Sci.* **2016**, *75*, 523. [[CrossRef](#)]
32. Goudie, A.S.; Brunnsden, D.; Collins, D.N.; Derbyshire, E.; Ferguson, R.J.; Jones, D.K.C.; Perrott, F.A.; Said, M.; Waters, R.S.; Whalley, W.B. *The Geomorphology of the Hunza Valley Karakoram Mountains Pakistan*; Cambridge University Press: Cambridge, UK, 1984; Volume 2, p. 410.
33. Miller, K.J. *The International Karakoram Project*; Cambridge University Press: Cambridge, UK, 1984; Volume 1.
34. Hewitt, K. Natural dams and outburst floods of the Karakoram Himalaya. *IAHS* **1982**, *138*, 259–269.
35. Owen, L.A. Mass movement deposits in the Karakoram Mountains: Their sedimentary characteristics, recognition and role in Karakoram landform evolution. *Z. Geomorphol.* **1991**, *35*, 401–424. [[CrossRef](#)]
36. Hewitt, K. Catastrophic landslides and their effects on the Upper Indus streams, Karakoram Himalaya, northern Pakistan. *Geomorphology* **1998**, *26*, 47–80. [[CrossRef](#)]
37. Gardezi, H.; Bilal, M.; Cheng, Q.; Xing, A.; Zhuang, Y.; Masood, T. A comparative analysis of attabad landslide on January 4, 2010, using two numerical models. *Nat. Hazards* **2021**, *107*, 519–538. [[CrossRef](#)]
38. Chen, X.; Cui, P.; You, Y.; Cheng, Z.; Khan, A.; Ye, C.; Zhang, S. Dam-break risk analysis of the Attabad landslide dam in Pakistan and emergency countermeasures. *Landslides* **2017**, *14*, 675–683. [[CrossRef](#)]

39. Shi, Y.; Wang, W. Research on snow cover in China and the avalanche phenomena at Batura Glacier, Pakistan. *Ann. Glaciol.* **1980**, *13*, 289–293. [[CrossRef](#)]
40. Hewitt, K. Catastrophic landslide deposits in the Karakoram Himalaya. *Science* **1988**, *242*, 64–67. [[CrossRef](#)]
41. Kuo, Y.-S.; Tsai, Y.-J.; Chen, Y.-S.; Shieh, C.-L.; Miyamoto, K.; Itoh, T. Movement of deep-seated rainfall-induced landslide at Hsiaolin Village during Typhoon Morakot. *Landslides* **2013**, *10*, 191–202. [[CrossRef](#)]
42. Comegna, L.; Picarelli, L.; Bucchignani, E.; Mercogliano, P. Potential effects of incoming climate changes on the behaviour of slow active landslides in clay. *Landslides* **2013**, *10*, 373–391. [[CrossRef](#)]
43. Martelloni, G.; Segoni, S.; Fanti, R.; Catani, F. Rainfall thresholds for the forecasting of landslide occurrence at regional scale. *Landslides* **2012**, *9*, 485–495. [[CrossRef](#)]
44. Prokešová, R.; Medved'ová, A.; Tábořík, P.; Snopková, Z. Towards hydrological triggering mechanisms of large deep-seated landslides. *Landslides* **2013**, *10*, 239–254. [[CrossRef](#)]
45. Shen, H.; Klapperich, H.; Abbas, S.M.; Ibrahim, A. Slope stability analysis based on the integration of GIS and numerical simulation. *Autom. Constr.* **2012**, *26*, 46–53. [[CrossRef](#)]
46. Huang, C.-C.; Yuin, S.-C. Experimental investigation of rainfall criteria for shallow slope failures. *Geomorphology* **2010**, *120*, 326–328. [[CrossRef](#)]
47. Schmertmann, J.H. Estimating slope stability reduction due to rain infiltration mounding. *J. Geotech. Geoenviron. Eng.* **2006**, *132*, 1219–1228. [[CrossRef](#)]
48. Zhang, X.; Shi, Y. *Changes of the Batura Glacier in the Quaternary and Recent Times*; Sinica, S.P.A., Ed.; Lanzhou Institute of Glaciology and Geocryology: Beijing, China, 1980; pp. 83–89.
49. Raschid, S. *Between Two Burrs on the Map—Travels in Northern Pakistan*; Vanguard Books Ltd.: Lahore, Pakistan, 1995.
50. van Westen, C.J.; Castellanos, E.; Kuriakose, S.L. Spatial data for landslide susceptibility, hazard, and vulnerability assessment: An overview. *Eng. Geol.* **2008**, *102*, 112–131. [[CrossRef](#)]
51. Corominas, J.; Moya, J. A review of assessing landslide frequency for hazard zoning purposes. *Eng. Geol.* **2008**, *102*, 193–213. [[CrossRef](#)]
52. Glade, T. Linking debris-flow hazard assessments with geomorphology. *Geomorphology* **2005**, *66*, 189–213. [[CrossRef](#)]
53. Kazmi, A.H.; Jan, M.Q. *Geology And Tectonics Of Pakistan*; Graphic Publishers: Karachi, Pakistan, 1997; p. 528.
54. Gaetani, M. The Karakorum Block in Central Asia from Ordovician to Cretaceous. *Sediment. Geol.* **1997**, *109*, 339–359. [[CrossRef](#)]
55. Desio, A. *Geologic evolution of the Karakorum & Geodynamic of Pakistan*; Milano, U.d.s.d., Ed.; Instituti di Geologica e Paleontologia: Milano, Italy, 1979; pp. 111–124.
56. Le Fort, P.; Pécher, A. An introduction to the geological map of the area between Hunza and Baltistan, Karakoram-Kohistan-Ladakh-Himalaya region, northern Pakistan, scale 1:150,000. *Geologica* **2002**, *6*, 1–199.
57. Searle, M.P. Geological evolution of the Karakoram Ranges. *Ital. J. Geosci.* **2011**, *130*, 147–159. [[CrossRef](#)]
58. Turner, A.; Schuster, R. *Landslides: Investigation and Mitigation: Transportation Research Board Special Report 247*; National Research Council: Washington, DC, USA, 1996; Volume 673.
59. ASTM. *Annual Book of ASTM Standards*; ASTM: West Conshohocken, PA, USA, 2010; Volume 00.01, p. 1689.
60. Stevens, J. Unified soil classification system. *Civ. Eng. Mag.* **1982**, *52*, 61–62.
61. Spencer, E. A method of analysis of the stability of embankments assuming parallel interstice forces. *Geotechnique* **1967**, *17*, 11–26. [[CrossRef](#)]
62. Swanson, H.E.; Morris, M.; Stinchfield, R.P.; Evans, E.H. *Standard X-ray Diffraction Powder Patterns*; National Bureau of Standards: Washington, DC, USA, 1962.
63. Rocchi, G.; Vacigato, G.; Callerio, A.; Fontana, M.; Previtali, R. Description of soils based on geomechanical criteria for improved landslide classification. *Landslides* **2013**, *11*, 813–825. [[CrossRef](#)]
64. Cook, D.; Santi, P.; Higgins, J. Prediction of piezometric surfaces and drain spacing for horizontal drain design. *Landslides* **2012**, *9*, 547–556. [[CrossRef](#)]
65. Rashid, M.U. Slope Stability Analysis of Maicher Landslide Upper Hunza, Gilgit Baltistan, Pakistan. Master's Thesis, University of Peshawar, Peshawar, KP, Pakistan, 2018.
66. Bittelli, M.; Valentino, R.; Salvatorelli, F.; Rossi Pisa, P. Monitoring soil-water and displacement conditions leading to landslide occurrence in partially saturated clays. *Geomorphology* **2012**, *173–174*, 161–173. [[CrossRef](#)]

**Disclaimer/Publisher's Note:** The statements, opinions and data contained in all publications are solely those of the individual author(s) and contributor(s) and not of MDPI and/or the editor(s). MDPI and/or the editor(s) disclaim responsibility for any injury to people or property resulting from any ideas, methods, instructions or products referred to in the content.